Constitutive Model for Thermal Compaction of Clayey Geomaterials and Application to COx Claystone

Mountaka Souley, M.-N. Vu, G. Armand, C. Plua

Constitutive model for thermal compaction of clayey geomaterials and application to COx claystone

M. Souley[1*], M.-N. Vu[2], G. Armand[3], C. Plua[3]

[1]Ineris, c/o Ecole des Mines de Nancy, Campus ARTEM, CS 14234, F-54042 Nancy Cedex, France

[2] Andra, 92298 Chatenay-Malabry, France

[3]Andra, Meuse/Haute-Marne Underground Research Laboratory, 55290 Bure, France

[*]Corresponding author: Mountaka.Souley@ineris.fr ; Tel: +33 3 54 40 66 33

Abstract

Clay formations present very favourable conditions for the long-term containment of radioactive waste due to their low hydraulic conductivity, high radionuclide retention capacity and limited fracturing in their natural state. But it is also due to the very low permeabilities of clays and claystone that drained conditions occur only at very slow temperature increases. The response is then partially drained or undrained with the consequence of thermal pressurisation induced by the thermal gradient. Furthermore, thermo-hydro-mechanical characterisations under drained and undrained conditions carried out on samples of the Callovo-Oxfordian (COx) clay formation and *in-situ* experiments performed by Andra at the Meuse/Haute-Marne underground research laboratory (LS M/HM) have also highlighted the strongly-coupled and complex thermo-hydro-mechanical processes of this material. In particular, the volume changes of the COx claystone subjected to a temperature rise under a constant isotropic stress close to the *in-situ* conditions of the LS M/HM laboratory in saturated and drained conditions, were highlighted. A behaviour comparable to that of over-consolidated clays depending on temperature is then experimentally observed, i.e., thermo-elastic expansion followed by thermoplastic contraction: the transition temperature between these two volumetric deformation mechanisms would correspond to the maximum temperature value undergone by the COx claystone during its geological history. Based on the extensive literature on the thermomechanical behaviour of clays and clayey soils, recent thermo-hydro-mechanical tests conducted on COx samples, as well as the database on the instantaneous behaviour of COx claystone, a constitutive model for the thermomechanical behaviour of COx claystone is proposed, then implemented in a commercial computation code. The transverse isotropic elastic and then elastoplastic instantaneous behaviour (beyond the elastic limit) up to the peak strength of the COx claystone, thermoplastic and hydrostatic compactions are taken into account. The model is first validated on triaxial and hydrostatic paths. The simulation of one of the drained hydrostatic stress heating tests performed by Braun et *al*. verified that the proposed model was able to reproduce the thermal compaction phenomenon highlighted by the authors and to show its operational character.

Highlights

• As for over-consolidated clays, the volume changes of COx claystone subjected to temperature rise, exhibit a thermoelastic expansion followed by thermoplastic compaction.

• The transition temperature between these two volumetric mechanisms would correspond to the maximum temperature undergone by the COx during its geological history.

• A thermoelastoplastic model is proposed by incorporating the observed nonlinear behaviour of the COx claystone up to its strength, with the two volumetric strain mechanisms.

• The proposed model is implemented in the commercial geomechanical software, *FLAC^{3D}*.

• After checking the model on triaxial stress paths, the drained hydrostatic stress heating tests performed by Braun et *al*. are used to validate the proposed model.

Keywords

THM behaviour, thermal compaction, thermoplastic behaviour, numerical implementation, numerical simulations

1 INTRODUCTION

Three clay formations in Europe have been studied in detail as potential host rocks for high-level radioactive waste disposal: the Boom clay in Belgium (Mertens et al. 2004), the Opalinus claystone in Switzerland (Bossart et al. 2002, 2004, Blümling et al. 2007) and the Callovo-Oxfordian (COx) clay formation in France (Armand et al. 2014). Thus, in the context of the potential creation of the radioactive waste storage project in the COx claystone (Cigéo), in-depth studies on the thermo-hydro-mechanical (THM) behaviour of the storage structures throughout their lifetime (from their construction to beyond their closure) have been underway for several years, and one of the issues is the description of the response of the host rock, the COx, for different situations representative of the behaviour of the various storage components. Thermo-hydro-mechanical characterisations in drained and undrained conditions on laboratory samples and the development of constitutive models have conducted in parallel with the *in-situ* experiments carried out by Andra at the Meuse/Haute-Marne (LS M/HM) underground research laboratory in the COx formation. In fact, in-situ heating tests have been undertaken to understand the thermal effects on the COx claystone at the Bure Underground Research Laboratory (URL): TER, TED, EPT, ALC1604, ALC1605 and CRQ tests (Wileveau and Su 2007, Conil et al. 2020, Armand et al. 2017a). The tests' scale varies from borehole with 76 mm of diameter (TER, TED, EPT), micro-tunnel with 0.8-1.0 m of diameter (ALC1604, ALC1605) to a representative HLW repository with several heating boreholes (CRQ, EPT). All these field tests showed that the sedimentary clays react to heat conduction with a raise of pore pressure and related mechanical effects. The measured results and numerical interpretations have led to better characterisation of THM properties and understanding of the THM behaviour of these clay formations (Gens et al. 2007, Garitte et al. 2014, Seyedi et al. 2017, Armand et al. 2017b).

But it is also due to the very low permeabilities of clays and claystone that drained conditions occur only at very slow temperature increases resulting in a partially drained or undrained response. Under these conditions and due to the strongly-coupled THM processes involved, the generation of pore pressure as a result of temperature increase (thermal pressurisation) leads to a decrease in effective stresses which can induce hydraulic fracturing and compromise the safety and performance of the storage. Thermal pressurisation occurs when saturated geomaterials are heated under undrained conditions (Ghabezloo and Sulem 2009, Tamizdoust and Ghasemi-Fare 2020). The higher thermal expansion of water compared to that of the solid skeleton induces an increase in pore water pressure. Laboratory studies have demonstrated this phenomenon in the COx claystone (Mohajerani et al. 2012, Zhang et al. 2017) and in the Opalinus claystone (Monfared et al. 2011). The thermal pressurisation mechanism thus represents an interaction between the solid and fluid phases, therefore the pore fluid properties play an important role, as shown by Baldi et al. (1988) on low porosity clays, Ghabezloo et al. (2009) on hardened cement paste, Monfared et al. (2011) on Opalinus claystone, or more recently Mohajerani et al. 2012, Zhang et al. 2017, Mohajerani et al. 2014, Belmokhtar et al. 2017, Braun 2019, Braun et al. 2019 on COx claystone.

In addition to this phenomenon of thermal pressurisation under the effect of thermal gradients in undrained conditions, the mechanism of plastic thermal compaction occurring above certain temperature thresholds on clay and shale soils and rocks is also of great importance. Several experimental studies have shown that heating a saturated clay sample under hydrostatic and drained conditions induces volume changes that depend on its consolidation history (Baldi et al. 1988, Hueckel and Baldi 1990, Towhata et al. 1993, Sultan et al. 2002, Cekerevac and Laloui 2004, Abuel-Naga et al. 2007, Monfared et al. 2011). These studies have highlighted the influence of temperature on the mechanical properties of clayey soils and rocks, and the mechanical behaviour of these clayey materials. These thermal effects manifest themselves in different forms: thermal softening (negative strain hardening) and/or hardening (positive strain hardening), changes in fluid pressure (pressurisation), changes in volume (thermo-elastic expansion, irreversible thermoplastic compaction) (Delage et al. 2000, Abuel-Naga et al. 2007, Mohajerani et al. 2012, Braun et al. 2019). Since the 1980s, several thermoplastic models have been developed for these clay soils and clays subjected to high temperatures (Mróz and Raniecki 1976, Hueckel and Borsetto 1990, Robinet et al. 1996, Cui et al. 2000, Laloui and Cekerevac 2003, François and Laloui 2008, Hamidi et al. 2015, etc.).

While some models are based on thermodynamic principles (Collins and Kelly 2002), many focus on the mechanical behaviour of clay materials based on isotropic critical state plasticity by extending (or not) the early work on the Cam-Clay model (Hueckel and Borsetto 1990, Cui et al. 2000, Hamidi and Khazaei 2010). Theoretical developments of coupled thermoplasticity have been reported in Simo and Miehe (1992); numerical implementations have been presented in Simo and Miehe (1992), Armero and Simo (1993), and the uniqueness of the thermoplastic solution has been discussed in Mróz and Raniecki (1976), Sloderbach and Pajak (2010).

Due to their lower permeability, there is very little data available on fully saturated and drained thermal tests on COx claystone. CERMES (Ecole des Ponts, Paris) has designed a special hollow cylinder triaxial apparatus to perform these difficult tests. In particular, the volume changes of the COx claystone subjected to a temperature rise under a constant isotropic stress close to the *in-situ* conditions of the LS M/HM URL in saturated and drained conditions, could be studied (Mohajerani et al. 2014, Menaceur et al. 2016, Belmokhtar et al. 2017, Braun 2019, Braun et al. 2019). The drained heating test conducted by Menaceur et al. (2016) indicated thermal contraction throughout the test, i.e. a behaviour comparable to that of normally-consolidated (NC) or low OCR (overconsolidation ratio) clays (Cekerevac and Laloui 2004, Delage et al. 2000). Conversely, in the tests conducted by Mohajerani et al. 2014 and Belmokhtar et al. (2017), a behaviour comparable to that of over-consolidated clays with increasing temperature was revealed, i.e. thermoelastic expansion followed by thermoplastic contraction: the transition temperature between the two mechanisms is 32 and 48°C respectively for Mohajerani et al. 2014 and Belmokhtar et al. (2017). On the Opalinus claystone, Monfared et al. (2011) observed an expanding/contracting behaviour with an (elastic) expansion up to a temperature of 65°C close to the estimated maximum temperature sustained during its geological history (65-70°C). The expansion was followed by a contraction at a higher temperature (up to 80°C). The physical mechanisms controlling this contraction are poorly understood, most authors believing that it is due to the release of adsorbed water within the clay part (Monfared et al. 2011, Braun 2019, Braun et al. 2019, 2020). In fact, this thermoplastic compaction mechanism observed on the clay samples is not in agreement with the *in-situ* measurements of thermally-induced pore pressure, which seemed to be correctly modelled with a thermoelastic assumption (Gens et al. 2007). The question is: if this thermoplastic compaction process really exists at the scale of the structure, what would the possible consequences be on the redistribution of stresses and on the evolution of stresses in heated zones sufficiently far from the waste storage galleries and remaining in a state of stress close to the initial one? Hence the need to develop an operational constitutive model for the numerical modelling of structures, taking into account the advances in knowledge of the mechanical and thermomechanical behaviour of this claystone.

Based on some experimental data on the THM behaviour of COx claystone, the abundant bibliography on the experimental characterisation of thermoplastic deformation mechanisms in clay soils, and the associated rheological behaviour essentially based on soil mechanics and the notion of limit state/critical state, we propose a constitutive model of the thermoplastic behaviour of claystone.

The first section is devoted to a state of the art on clays and clayey soils, on the one hand, on the mechanisms that may occur following a rise in temperature and that depend on the degree of consolidation (maximum supported stress) and maximum temperature that the rock has endured during its history; and, on the other hand, on the constitutive models of thermomechanical behaviour of clays and clayey soils found in the literature. On this basis, the second section focuses on a proposed thermoplastic behaviour model for claystone and its numerical implementation in the commercial geomechanical software, *FLAC^{3D}*. The proposed model is subsequently applied to reproduce triaxial tests performed on the COx claystone (Armand et al. 2017c). An example of hydrostatic behaviour simulation is also presented: this allows for the verification of the model on isotropic stress paths. Finally, the last example simulates the test of Braun et al. (2020, 2021). The ability of the proposed model to reproduce the observed thermal compaction beyond the maximum temperature values reached during the thermal history of the COx claystone is discussed.

2 LITERATURE REVIEW

2.1 Volumetric thermoplastic behaviour - experimental data synthesis

These studies have highlighted the influence of temperature on the behaviour and mechanical properties of clayey soils and rocks (Baldi et al. 1991, Delage et al. 2000, Abuel-Naga et al. 2007, Mohajerani et al. 2012, Braun et al. 2019). Specifically for these clay geomaterials, temperature

influences the pre-consolidation stress through a decrease with increasing temperature (Sultan et al 2002, Cekerevac and Laloui 2004), compressibility and swelling index (Cui et al. 2000), strength and/or slope of the critical state line (Cekerevac and Laloui 2004). According to the work of Cui et al. (2000, 2009), the compression and swelling indices (deduced from the oedometer curves) for Boom clay are not affected by temperature when the stress level is relatively low (<1 MPa), but at higher stresses, Sultan et al. (2002) showed that the compression index at different temperatures converges to a value when the total stress increases. Cekerevac and Laloui (2004) report that shear strength may or may not vary due to thermal loading depending on the clay material, notably through studies on kaolin. Tests on underground storage clays and claystone (Boom, Opalinus and COx) show a slight decrease in shear strength for Boom clay (Hueckel et al. 2009), a significant decrease for Opalinus clay (Zhang et al. 2007, Zhang et al. 2019), and no significant change for COx claystone. Similarly, in the synthesis by Zhang et al. (2017), the strength envelopes at different temperatures are close to each other, indicating a non-significant influence of temperature on strength.

For Hueckel et al. (2009) and more generally, the evolution of the load area and the slope of the critical state line depend on the nature of the material, on its state with respect to the applied stress (OCR versus NC), the thermal history as well as on the test conditions (drained or undrained). The degree of over-consolidation (OCR) is known to have a major effect on the volume change of heated soil under constant load. At low OCR values, heating induces thermal contraction (Paaswell 1967). During heating of an NC sample, its volume change is non-linear. The behaviour over a full cycle indicates the irreversibility of volumetric deformation due to thermal loading resulting in thermal hardening. Even if there is no physical change in the effective stresses, this can be interpreted as though the material underwent densification. On the contrary, at high OCR values, heating results in thermal expansion (Baldi et al. 1988, Towhata et al. 1993).

More specifically, heating tests performed on Boom clay by several authors (Baldi et al. 1991, Cekerevac and Laloui 2004) indicate that the volumetric behaviour depends on the OCR. For normally-consolidated samples (or low OCRs), a contracting behaviour of the sample during heating is observed (Sultan et al. 2002, Cekerevac and Laloui 2004, Delage et al. 2000) as illustrated in Figure 1. This is also the same behaviour observed on some COx claystone samples by Mohajerani et al. (2014) (thermal contraction of the COx sample during a drained heating test under a constant isotropic stress close to the *in-situ* LS M/HM laboratory conditions of 12 MPa and a pore pressure of 4 MPa) and by Menaceur et al. (2016).

On the other hand, on over-consolidated clays, a transition between thermoelastic expansion and thermoplastic contraction is observed by Baldi et al. 1988, Delage et al. 2000, Sultan et al. 2002 on Boom clay for OCRs of 2 and 12 as illustrated in Figure 1, by Cekerevac and Laloui 2004 on kaolin clay with an OCR of 12, and by Abuel-Naga et al. (2007) on over-consolidated Bangkok clay. For the latter, heating of the normally-consolidated samples induced non-reversible volume changes upon cooling (i.e. irreversible plastic behaviour) as in the case of Boom clay in Figure 1.

For Boom clay, drained tests at several degrees of consolidation and effective stresses have shown (Cui and Tang 2013) that: (a) the thermal contraction on a normally-consolidated sample is independent of the mean effective stress, and this is also true for OCR=12; (b) the thermal contraction increases when the OCR decreases, leading to pure contraction at OCR=1 in agreement with the results of Baldi et al. (1988); (c) the slope of the volumetric strain during the cooling phase is independent of the mean effective stress; (d) and the temperature at which the volumetric expansion/compaction transition occurs decreases with the OCR (T=80°C at OCR=12, 50°C at OCR=2) in agreement with the tests of Baldi et al. (1988) and Towhata et al. (1993). In addition, the cooling slopes are parallel to the elastic expansion during loading.

For claystone, there is little data available on the subject. Monfared et al. (2011) have highlighted the thermal hardening process in the Opalinus claystone, with thermoelastic expansion up to a temperature of 65°C (this threshold value of 65°C appears to be a plausible maximum temperature that the formation would have undergone in the course of its geological history) followed by a contraction for heating up to 80°C (Figure 2). During the heating/cooling cycle, the behaviour of the sample is elastic contraction during the cooling phase. This behaviour is therefore similar to that of over-consolidated clays with a low OCR. For the second heating cycle up to 80°C, thermal expansion is observed, showing a thermal hardening phenomenon.

The work of Belmokhtar et al. (2017) has also assessed the role of temperature on the instantaneous and delayed volumetric behaviour of COx claystone. The transition between thermoelastic dilatation

and thermoplastic contraction in Figure 3 is typical of the over-consolidated clays discussed previously (for example, Baldi et al. 1988, Sultan et al. 2002 on Boom clay, Abuel-Naga et al. 2007 on Bangkok clay, and Monfared et al. 2011 on Opalinus claystone). This is also the same behaviour observed by Mohajerani et al. (2014) on COx samples heated under drained conditions and stresses prevailing *in situ* (12 MPa) but previously subjected to a higher stress state than *in situ* (18 MPa). The temperature at which the transition between thermal expansion and thermoplastic contraction occurred is close to the maximum burial temperature of the COx claystone, estimated at 50°C. Recall that Blaise et al. (2014) estimated a maximum temperature value of 50 ± 5°C to which the COx claystone would have been exposed during its history. This means that the claystone retains the memory of the highest exposure temperature, below which it exhibits thermoelastic expansion. In other words, temperature has an effect comparable to that of stress in the consolidation process of clayey soils and rocks, with an elastic response in a temperature range already supported, followed by elastic and plastic contraction when this limit is exceeded, exhibiting thermal hardening behaviour. This is consistent with existing thermoplastic models that provide a definition of an elastic zone and a yielding surface in the (p', T) plane, e.g. Hueckel and Borsetto (1990), Sultan et al. (2002).

Mohajerani et al. (2014) also observed this trend under *in-situ* stress conditions on COx samples subjected to heating, i.e. a transition between thermoelastic expansion between 25 and 32°C, followed by thermoplastic contraction between 32 and 80°C. Heating tests under drained and undrained conditions in the presence of a deviatoric stress performed by Zhang (2018) also showed this transition (thermoelastic expansion and thermoplastic contraction) but at much higher transition temperature values. This suggests a range of variability in the transition temperature between the two thermal mechanisms.

Finally, the work of Braun and co-authors (Braun 2019, Braun et al. 2019, 2020, 2021) has also advanced the understanding of the THM behaviour of COx claystone experimentally, by performing the same tests (isotropic and drained under *in-situ* stress and pore pressure conditions, as in the previous studies) with samples cored parallel and perpendicular to the layering plane (Figure 4). For samples parallel to the bedding, the response to the temperature cycle is reversible. Conversely, for samples oriented perpendicularly, the results are similar to the observations of Belmokhtar et al. (2017), who observed thermal expansion up to 50°C (the highest temperature value experienced during the geological history estimated by Blaise et al. 2014 for COx claystone), followed by contraction at higher temperatures. The plastic part of the observed thermo-elasto-plastic volumetric response was mainly due to deformations perpendicular to the bedding, where the authors suspect a link with absorbed water while thermoelastic deformations parallel to the bedding correspond to thermal expansion of its minerals. To describe this contraction (thermal compaction), Braun et al. (2019, 2020, 2021) define an elastoplastic drained expansion coefficient, $\alpha^*_{d,z}$:

$$\alpha^*_{d,z} = \alpha_{d,z} + \alpha^p_{d,z} \quad (1)$$

which comprises a reversible part $\alpha_{d,z}$ and an irreversible one $\alpha^p_{d,z}$. Therefore, based on Figure 4, Braun et al. (2021) propose a linear relationship between $\alpha_{d,z}$ and $\alpha^p_{d,z}$ depending on the temperature between 25 and 90°C for the (perpendicular) ISO3 and ISO4 samples.

With regard to the effect of temperature on the mechanical properties of COx claystone, Menaceur et al (2016) in a large experimental programme investigated the effect of temperature on shear strength and volume changes under saturated and drained conditions. Shear tests at temperatures above 80°C showed little change in elastic parameters with the temperature, confirming the results of Mohajerani et al. (2014). Preliminary results obtained on the COx claystone showed a more ductile response and slightly lower shear strengths at high temperatures, in agreement with the few published data available on claystone (Menaceur et al. 2016, Zhang et al. 2017) and shales. Subsequently, and as a first approach, we then assume that the yield strength, the peak strength of COx claystone and more generally the yield surfaces during work hardening are not temperature dependent. Furthermore, the thermomechanical behaviour will be ductile limited to the pre-peak phase of the COx claystone behaviour, as suggested by tests at high temperatures.

2.2 Some constitutive models for clays

Over the last few decades, several experimental studies on the behaviour of clay and clayey soils depending on temperature have been carried out. These studies have shown that temperature modifies both the physical and mechanical characteristics of the soil. Based on these observations,

many thermomechanical models capable of representing the main characteristics of clays under thermal gradients have been developed (Hueckel and Borsetto 1990, Robinet et al. 1996, Cui et al. 2000, Hamidi and Khazaei 2010, Yao and Zhou 2013, Xiong et al. 2017, Bellia et al. 2015, Hamidi et al. 2015, Hong et al. 2016, Hamidi and Tourchi 2017, etc.). Many of these models go beyond the standard or modified Cam-Clay model.

Hueckel and Borsetto (1990) studied the plastic behaviour of clays under isothermal conditions. They found that the yield strength is temperature dependent and decreases with increasing temperature. Robinet et al. (1996) used the modified Cam-Clay model to propose a thermo-elasto-plastic model for saturated clays with two distinct plastic mechanisms: one purely thermal, which results in negative strain-hardening of irreversible thermal deformations, and the second thermo-mechanical, where the yield surface and strain-hardenings depend on temperature The originality of this model, compared to the previous one, is the introduction of irreversible thermal deformations which control the thermal softening. This mechanism, which is accentuated in drained and over-consolidated conditions, is observed on tests carried out by several authors.

Based on the Boom clay tests, some results of which have been mentioned above, and on data from different soils, obtained separately by different authors, Cui et al. (2000) developed an elastoplastic model, extending the work of Hueckel and Borsetto (1990), which helps describe the thermo-elastoplastic behaviour. The proposed model includes: (a) a plastic volumetric mechanism capable of modelling plastic deformations at high OCRs; (b) the over-consolidation effect observed when heating a normally-consolidated soil; and (c) the coupling and strain-hardening phenomena under the combined effect of temperature and stress (mechanical loading). In this model, particular attention was paid to the coupling and strain-hardening phenomena related to the combined effects of stress and temperature. The deviatoric stress effects in this model by Cui et al. (2000) are taken into account using the standard Cam-Clay approach. The contribution of Hong et al. (2016) enhances the work of Cui et al. (2000) by emphasising some important thermomechanical features of natural clays that have been experimentally demonstrated, such as a limited thermomechanical elastic zone, a smooth transition between elastic and plastic behaviour. Two plastic mechanisms are introduced in the model: the first consists of reproducing the thermoplasticity involving thermal expansion and contraction observed at high over-consolidation rates, and the second describes the effect of temperature on the elastic behaviour. Finally, the model is validated by simulating experimental tests on Boom clay along different thermomechanical paths. Recently, this model has been extended to the thermoporoplasticity of saturated clays under undrained conditions (Cheng et al. 2020).

The models developed by Laloui and co-authors are based on the main mechanisms described above, to which are added: (a) a deviatoric mechanism based on an extension of the Cam-Clay model in which the slope of the critical state limit (or friction coefficient) depends on the temperature. This deviatoric mechanism is improved by performing a cut-off at tensile strength in the (q, p') plane where q and p' denote the deviatoric stress and the mean effective stress respectively; (b) the oedometer moduli (compressibility and swelling) are temperature dependent through the pre-consolidation stress; (c) an isotropic thermoplastic mechanism represented by a non-linear envelope in the (p', T) plane. The mathematical formulation, details of the constitutive equations for numerical implementation and validation tests of the latest version of their model called ACMEG-T (Advanced Constitutive Model for Environmental Geomechanics-Thermal effect) is given in François and Laloui (2008). The plastic flow rule is associated and non-associated respectively for the hydrostatic and shear mechanisms. Finally, the strain hardening parameter that defines the increase (hardening) or decrease (softening) of the yield surface for the hydrostatic mechanism is the pre-consolidation stress p'_c of which an expression often used in the literature was proposed by Laloui and Cekerevac (2003):

$$p'_{c0}\left(1-\gamma log\left(\frac{T}{T_{ref}}\right)\right)e^{\tilde{\beta}\varepsilon_v^p} \qquad (2)$$

where p'_{c0} is the isothermal value of the initial pre-consolidation stress, $\tilde{\beta}$ the plastic compressibility, ε_v^p the accumulated volumetric plastic strain (compressive stress and strain are positive), γ a material parameter representing the softening rate, T and T_{ref} the current and reference temperature, respectively.

This ACMEG-T model has been validated on heating tests conducted on Boom, Kaolin and Opalinus clays. The model is implemented in the finite element code LAGAMINE (Collin et al. 2002) by François et al. (2009) and later by Hueckel et al. (2011), which allowed the authors to carry out a THM

application of the constitutive model by simulating the large-scale ATLAS heating experiment at the underground HADES-URF laboratory in Mol (Belgium) in Boom clays.

Thus, most of the rheological models of clays and clayey soils were based on the concept of the critical limit state theory which is not common in the field rock mechanics and rock engineering. Therefore, their formulation explicitly involves the pre-consolidation stress p'_c which allows the hydrostatic yield to be controlled through the variations of the void index: it depends on the volumetric deformation (contraction or expansion depending on the mechanism involved), the temperature and/or the degree of consolidation (OCR). One of the forms widely used in the literature (Semnani et al. 2016, Zhao et al. 2018, Borja et al. 2020) is the that proposed by Laloui and Cekerevac (2003) recalled in equation (3). The general form of the expression of the pre-consolidation stress is as follows:

$$p'_c = p'_{c0}\, exp\left(\frac{\varepsilon_v^c}{\lambda^p}\right) \Theta_1(T) + \Theta_2(T) \tag{3}$$

where p'_{c0} is the value of the pre-consolidation stress at the reference temperature, T_{ref} ; $\lambda^p = C_c$ - C_r ; $C_r > 0$ elastic compressibility index; $C_p (> C_r)$ total compressibility index; ε_v^c volumetric deformation associated to the compaction mechanism (case of thermal compaction); $\Theta_1(T)$ and $\Theta_2(T)$ are two author-dependent thermal strain hardening (softening and/or hardening) functions. Table 3 provides some expressions of $\Theta_1(T)$ and $\Theta_2(T)$ reported in the literature.

Some models take into account the coupled behaviour, including thermal, viscous, hydraulic, chemical and mechanical aspects (e.g. Liu et al. 2007, Chen et al. 2007, Yao and Zhou 2013, Hamidi et al. 2015, Geng et al. 2020, Borja et al. 2020). Recently, studies have been conducted on the thermo-hydro-mechanical behaviour of partially-saturated clay soils (Khalili and Loret 2001, Romero et al. 2003, François and Laloui 2008, Bellia et al. 2015, Hamidi and Tourchi 2017).

As we have just seen, a large number of models for clay soils have been proposed based on the modified Cam-Clay model. In order to overcome some of their drawbacks (Gens and Potts 1988), such as overestimation of dilatancy (Lagioia and Potts 1988), overestimation of the shear strength of over-consolidated clays and abrupt transition from elasticity to plasticity, boundary surface models (e.g. Dafalias 1986, Bellia et al. 2015) and internal yield surface models (e.g. Chakraborty et al. 2013, Hong et al. 2016) have been developed. However, these models are still not commonly used in engineering practice due to their complexity. In an attempt to avoid this gap between sophisticated academic models and models used in engineering practice, Rachdi et al. (2019) propose a model that is in line with the perspective of correcting the overestimation of maximum strength and prediction of expansion based on the concept of boundary state, a non-associated flow rule and two mechanisms (shear and compaction). This model was validated for normally-consolidated and over-consolidated clays. The coupling between the shear mechanisms and volumetric strain hardening was verified on a series of specific triaxial tests with controlled stress paths on an over-consolidated natural grey marl. In the same vein, Samudio (2018) proposes an alternative to the modified Cam-Clay model. This model called asymmetric Cam-Clay is isotropic and accounts for a transition between volumetric contraction and dilatancy. It is expressed in terms of stress invariants with an elastic limit of elliptical type.

3 NEW THERMO-ELASTO-PLASTIC MODEL FOR COX CLAYSTONE

3.1 Main assumptions

Here we recall the main assumptions and key points from which we have been inspired to develop a constitutive model for the thermoplastic behaviour of claystone:

- The model is built in the framework of elastoplasticity theory.
- The model is written in the framework of infinitesimal transformations. The total strain tensor is therefore considered to be the sum of the elastic strain tensor, the plastic shear strain tensor and plastic strains resulting from crushing (“pore collapse”) / densification (compaction of cement between grains, crushing of grains): the elastic deformations are themselves decomposed into a mechanical part (Hooke's law) and a reversible thermal part.
- The medium is considered to be homogeneous, elastically transverse isotropic and plastically isotropic (as a first approach).

- The plastic shear mechanism common to most materials with internal friction is also considered. Plastic deformation is induced by sliding “crystalline lattices” and contact surfaces between grains.

- The model will be limited to the non-linear elastoplastic behaviour of the claystone in pre-peak regime, i.e. up to the peak strength. This allows us to reproduce the ductile feature observed in the COx claystone under high temperatures. Subsequently, if necessary, the work will be extended to the post-peak behaviour. The model selected will therefore include an elastic phase, a non-linear plastic phase between the elastic limit and the peak, and a plateau equal in value to the peak strength of the COx claystone. The yielding surface expressed in (p’, q, θ) is non-linear and dependent on the Hoek-Brown parameters whose values at the elastic limit and at the peak are well identified (Su 2003, Armand et al. 2017c).

- It is generally observed on geomaterials that the shear mechanism may induce volumetric plastic deformations of contraction and/or dilatancy. We will assume this feature in this model. This justifies the choice of a non-associated flow rule (Chiarelli et al. 2003, Hoxha et al. 2004, Souley et al. 2017).
- As suggested by several laboratory observations (Menaceur et al. 2016, Zhang et al. 2017), we will assume that the elastic and strength characteristics (compressive and tensile) are temperature independent.
- The mechanism of collapse of the porous structure and "thermal compaction" explicitly involves the plastic volumetric strain and the pre-consolidation stress, which in turn depends on the temperature from a certain critical temperature or transition temperature between the thermoelastic expansion and plastic compaction, T_c. We will rely on the work hardening function proposed in the literature, the general form of which is given by the relation (3). It will be assumed that for temperatures and consolidation stresses such as $T < T_c$ and $p'_c < p'_{c0}$ then only the reversible thermoelastic expansion or contraction mechanism will be active. For temperatures and consolidation stresses such as $T \geq T_c$, $\dot{T} > 0$ and $p' \leq -p'_c$ then the mechanical pore collapse and thermoplastic compaction mechanisms will be active. As for tensile failure, we will adopt an associated flow rule for the mechanical pore collapse (or hydrostatic compaction) mechanism for the purposes of simplicity.
- We adopt the rock mechanics or continuum mechanics sign convention: compressions are counted negatively.

3.2 Thermoplastic volumetric deformation mechanism

For hydrostatic and thermal compactions (closed or cap yield surfaces), we adopt a simple yield surface instead of either (a) an elliptical shape (adaptation and generalisation of the Cam-Clay model) for clays and clayey soils and rocks or (b) the well-known Gurson ductile damage model which is the first physically based model, introducing an interaction between plastic deformation and cavity growth introduced by Rice et Tracey (1969). One of the most famous versions of this model is the GTN model (Gurson 1977 - Tvergaard and Needleman 1984), which deals with the nucleation, growth and coalescence stages of cavities. Subsequently, a number of rheological models have been developed for porous rocks (chalk, limestone) or for concrete based on this GTN model.

In the absence of experimental data concerning the failure of COx claystone according to hydrostatic loading paths, the isotropic yielding surface (crushing and densification of the rock) has been chosen as a first approach. If necessary, and if more experimental evidence is available, this formalism can be revisited later with several rheological models developed in the literature for porous rocks or concrete. It is therefore simply a cut-off on hydrostatic paths, isothermal or not:

$$F_c = -p' - p'_c(T, \varepsilon_v^c) \tag{4}$$

with T the temperature, ε_v^c the volumetric deformation of mechanical crushing and/or thermal compaction.

For double strain hardening in T and ε_v^c, we adopt the formulation of Picard (1994) taken up by Hong et al. (2016), in which we introduce the transition temperature between thermoelastic response (expansion) and thermoplasticity (compaction in the case of claystone), T_c:

$$\begin{cases} p'_c(T,\varepsilon_v^c) = p'_{c0}\, exp(-\vartheta\varepsilon_v^c) & if\ \ T < T_c\ \ or\ \ \dot{T} \le 0 \\ p'_c(T,\varepsilon_v^c) = p'_{c0}\, exp\left(-\vartheta\varepsilon_v^c - 3\alpha_T^p(T-T_c)\right) & if\ \ T \ge T_c\ \ and\ \ \dot{T} > 0 \end{cases} \quad (5)$$

where p'_{c0} is the initial consolidation pressure, p'_c the current consolidation pressure; T temperature, ϑ a strain hardening coefficient which is merely the plastic compressibility coefficient in the expression proposed by Laloui and Cekerevac (2003), α_T^p a positive scalar coefficient, having the dimension of a thermal expansion coefficient. It may be viewed as a "plastic" thermal expansion coefficient, whose negative values will be associated with irreversible thermal expansion and positive values with plastic compaction. Introducing the critical temperature as an input parameter makes it possible to reproduce both types of temperature-induced volumetric behaviour: (a) absence of thermoplastic threshold (Mohajerani et al. 2014, Menaceur et al. 2016), (b) thermoelastic expansion followed by thermoplastic contraction (Mohajerani et al. 2014, Belmokhtar et al. 2017, Braun 2019, Braun et al. 2019; 2020). The latter expression remains in the spirit of the thermoplastic behaviour of COx claystone illustrated in Figure 3 and Figure 4, i.e. a temperature cut-off at T_c and p'_c which would tend towards zero at very high temperatures.

In order to reduce the number of parameters of the constitutive model and in the absence of experimental data on the double strain hardening represented by equations (4) and (5), we will consider an associated flow rule, i.e.:

$$G_c = F_c = -p' - p'_c(T,\varepsilon_v^c) \quad (6)$$

We will therefore retain the same yield surface and plastic potential for the crushing mechanism (pore collapse) due to mechanical loading.

3.3 Elastoplastic shear mechanism

From laboratory tests carried out on samples of the COx claystone, the main features of the short-term behaviour are (Armand et al. 2013, Armand et al. 2017c): (a) a short linear elastic behaviour under low deviatoric stresses; (b) a nonlinear strain hardening by the appearance of plastic strains for low deviatoric stresses and prior to peak strength; (c) a post-peak strain softening behaviour which is brittle under low confining pressures and becomes ductile at high confinements; and finally (d) a purely frictional residual behaviour governed by the induced macro-cracks. In relation to the most ductile thermoplastic behaviour observed under high temperature, the instantaneous post-peak behaviour of the COx claystone is herein ignored.

As a result of the extensive experimental laboratory characterisations and *in-situ* investigations, several phenomenological elastoplastic, elastic-viscoplastic and damage models were initially proposed in the framework of irreversible thermodynamics. Some of these models were evaluated and compared with each other as part of a benchmark exercise for numerical analysis of the COx claystone hydromechanical response to excavation operations (Seyedi et al. 2017). Since then, some of these models have been enriched to address new advances in the understanding of COx behaviour or the regularisation of post-peak behaviour.

In addition, it has been shown that a failure criterion based on the Hoek-Brown criterion is well adapted to describe the shear strength of the Callovo-Oxfordian claystone, even if in their natural state they have no tectonic fractures. The generalisation of classical failure criterion of Hoek–Brown (1980) in the space of three stress invariants (p, q, θ) leads to the following criterion for plasticity initiation (or elastic limit) and peak strength and more generally for the shear yield surface (Souley et al. 2017):

$$F_s = \frac{4}{3}cos^2\,\theta\, q^2 + A\left(\frac{cos\,\theta}{\sqrt{3}} - \frac{sin\,\theta}{3}\right)q + Ap' - B \quad (7)$$

where p' represents the mean effective stress, q the generalised deviatoric stress and θ the Lode's angle, A and B are two independent parameters (A = m σ_c and B = s σ_c^2, evaluated at the elastic limit and peak, where m, s are the Hoek-Brown parameters and σ_c the uniaxial compressive strength).

In this relationship, the geometry of the stresses is considered through the Lode's angle. As a result, the failure criteria can be differentiated according to the compression paths (θ = π/6) and extension ones (θ = -π/6) as suggested by laboratory tests carried out on claystone samples.

The strain hardening is modelled as a non-linear change (cubic spline) of A with respect to the internal flow (plastic) variable from the initiation A_i to the peak A_p. We also considered a parabolic evolution of parameter B as a function of the internal plastic variable, with horizontal tangent at peak.

It is known that for most geomaterials, a non-associated flow rule is generally required to reproduce the transition between the plastic volumetric compressibility (contraction) and dilation. The following plastic potential based on Drucker-Prager form is adopted:

$$G_s = q + \beta\left(\varepsilon_s^p\right) p' \tag{8}$$

where ε_s^p (the internal flow variable) is the plastic distortion (or shear plastic strain), varies between a minimum value β_0 and a maximum value β_m. $\beta\left(\varepsilon_s^p\right)$ is the dilatancy rate (or coefficient) that its evolution is based on Souley et al. (2022) and given by:

$$\beta\left(\varepsilon_s^p\right) = \begin{cases} \beta_m - (\beta_m - \beta_0)e^{-b_\beta \varepsilon_s^p} & \varepsilon_s^p \le \gamma^{ult} \\ \beta_{ult} e^{\left(1 - {\varepsilon_s^p}/{\gamma^{ult}}\right)} & \varepsilon_s^p > \gamma^{ult} \end{cases} \tag{9}$$

where b_β is the plastic flow velocity, $\beta_{ult} = \beta_m - (\beta_m - \beta_0)e^{-b_\beta \gamma^{ult}}$.

Under large deformation field, it can be physically expected that the dilatancy will disappear reflecting a purely frictional behaviour. In order to account for this frictional response, a loss of dilatancy is then admitted. The ultimate shear plastic strain from which dilatancy decreases is noted γ^{ult}. Beyond this plastic deformation, the dilatancy rate gradually changes to tend asymptotically to zero.

3.4 Elastoplastic tensile mechanism

The tensile mechanism is limited by the Rankine criterion with a tensile strength σ_t, which in practice may be lower than that estimated from the Hoek-Brown criterion, i.e. a tensile strength under triaxial conditions, ${}^{s}\sigma_c/_m$. This will be a "cut-off" in σ_t with an associated flow rule. The yield surface and plastic potential for the tensile failure mechanism are expressed as follows:

$$F_t = p' - \sigma_t \tag{10}$$

where p' is the average effective stress (compressive stresses are counted negatively).

$$G_t = p' \tag{11}$$

Tensile strengths are those deduced from the Hoek-Brown criterion in triaxial configuration, i.e.: ${\sigma_t}^k = {}^{s_k}{\sigma_c}^k/_{m_k}$ where k = i (initiation) or p (peak) and ${\sigma_t}^i = minimum\left({}^{s_i}{\sigma_c}^i/_{m_i}, {}^{s_p}{\sigma_c}^p/_{m_p}\right)$.

3.5 Graphical representation of the proposed model and input parameters

An illustration of the different mechanisms involved in the proposed constitutive model is shown in Figure 5 in (q, p', T) space. The shear yield surface is of the Hoek-Brown type, expressed in the space of the 3 stress invariants. It evolves from the elastic limit to the peak strength. The projections of the yield surfaces in the (p', q) and (p', T) planes are shown in Figure 6. It has been assumed, in the absence of experimental data, that the consolidation stress equal to p'_{c0} remains constant for temperatures below T_c, i.e. a cut-off of p'_c in temperature. Figure 6a shows the three failure mechanisms that can occur individually or in a combined mode of thermal compaction/shear failure or tension/shear failure.

The model parameters for the shear and tensile mechanisms consist of:

- Hoek-Brown parameters at the elastic limit $(m_i,\ s_i, {\sigma_c}^i)$ and peak $\left(m_p,\ s_p, {\sigma_c}^p\right)$ and the tensile strengths at the yield point and peak $({\sigma_t}^i, {\sigma_t}^p)$;
- the initial and maximum expansion rate, $(\beta_0,\ \beta_m)$ its rate of evolution as a function of plastic deformation b_β as well as the ultimate plastic strain γ^{ult} at which the sample dilatancy stops growing.

All parameters have already been identified from triaxial tests for the short-term response (Su 2003, Chiarelli et al. 2003, Armand et al. 2017c, Souley et al. 2017). Note that COx claystone is a natural material with small mineral heterogeneity, so the results of laboratory tests showed a wide variability of elastic limit, the peak and residual strengths. Indeed, the interpretation of experimental data according to the parabolic criterion of Hoek-Brown (1980), usually used in rock mechanics, has allowed to propose two sets of parameters (m, s, σ_c) for the elastic limit, peak and residual criteria: one called "medium" that passed in the middle of the experimental data and the other "lower" which represents the lower bound of the experimental points (Su 2003). According to the purpose of this paper, the mean values of the parameters s_i, ${\sigma_c}^i$, m_i, s_p, ${\sigma_c}^p$, and m_p for elastic limit and peak strength are used (Table 2).

Hoek-Brown parameters, dilatancy and plastic strains at the initiation and peak thresholds were identified from the tests presented in Armand et al. (2017c). Three triaxial tests at confining pressures of 2, 6 and 12 MPa are used for identifying parameters. The resulting criteria for initiation and peak strengths are noted as the median to the mean and lower criteria expressed in terms of Hoek and Brown (1980).

For the thermal compaction mechanism with temperature threshold and consolidation stress, although the available experimental data on clays do not allow conclusions to be drawn on a temperature-dependent shear mechanism, we will assume that:

- the existence of pre-consolidation stress at the reference temperature $\boldsymbol{p'_{c0}}$. In rock mechanics, it corresponds to the pore collapse threshold in hydrostatic tests. In the absence of confirmed experimental data from hydrostatic tests on COx claystone, we consider it to be close to the average stress *in situ*: 11 MPa;
- the plastic compressibility and the thermal coefficient of plastic expansion α_T^p are to be determined from several isothermal hydrostatic tests at different temperature values. For COx claystone, a value of 850 was proposed by Braun et al (2021). We back-determined the value of $6\text{x}10^{-3}$ of α_T^p from the test of Braun et al. (2020);
- the transition temperature between thermoelastic expansion and thermoplastic contraction T_c observed on the tests of Belmokhtar et al. (2017), Braun et al. (2019, 2020, 2021) is close to the maximum burial temperature of the COx claystone, estimated at 50°C by Blaise et al. (2014). This value of T_c has been used here.

Finally, the average transverse isotropic thermoelastic parameters of the COx claystone from the laboratory characterizations are given in Table 3.

4 NUMERICAL IMPLEMENTATION AND VERIFICATION

4.1 Constitutive equations derivation

The deformation repartition rule (small perturbation assumption) makes possible to decompose the increment of the total strain tensor $d\underline{\varepsilon}$, into an elastic part $d\underline{\varepsilon}^e$ and an irreversible plastic part $d\underline{\varepsilon}^p$, which in turn is subdivided into hydrostatic, shear and tensile parts $\left(d\underline{\varepsilon}^c,\ d\underline{\varepsilon}^s,\ d\underline{\varepsilon}^t\right)$:

$$d\underline{\varepsilon} = d\underline{\varepsilon}^e + d\underline{\varepsilon}^p = d\underline{\varepsilon}^e + d\underline{\varepsilon}^c + d\underline{\varepsilon}^s + d\underline{\varepsilon}^t \qquad d\varepsilon_{ij} = d\varepsilon_{ij}^e + d\varepsilon_{ij}^c + d\varepsilon_{ij}^s + d\varepsilon_{ij}^t \tag{12}$$

where $d\varepsilon_{ij}^s$, $d\varepsilon_{ij}^t$ and $d\varepsilon_{ij}^c$ are respectively the increments of the irreversible deformations associated with the shear mechanism, the tensile failure and the pore collapse mechanism (induced by mechanical loading) and the thermal compaction mechanism. This results in:

$$d\varepsilon_{ij}^e = d\varepsilon_{ij} - \left(d\varepsilon_{ij}^c + d\varepsilon_{ij}^s + d\varepsilon_{ij}^t\right) = d\varepsilon_{ij} - \left(\lambda_c \frac{\partial G_c}{\partial \sigma_{ij}} + \lambda_s \frac{\partial G_s}{\partial \sigma_{ij}} + \lambda_t \frac{\partial G_t}{\partial \sigma_{ij}}\right) \tag{13}$$

$$d\varepsilon_{ij}^e = d\varepsilon_{ij} - \lambda_c \frac{\partial G_c}{\partial \sigma_{ij}} - \lambda_s \frac{\partial G_s}{\partial \sigma_{ij}} - \lambda_t \frac{\partial G_t}{\partial \sigma_{ij}} \tag{14}$$

where λ_c, λ_s and λ_t are the plastic multipliers associated with the pore collapse/thermal compaction mechanism, shear and tensile failures, respectively.

If $\underline{\underline{C}}$ represents the transverse isotropic tensor of elasticity, Hooke's law allows the **effective stress** increments $\left(d\underline{\sigma}\right)$ to be related to the elastic strains:

$$d\underline{\sigma} = d\sigma_{ij} = \underline{\underline{C}} : d\underline{\varepsilon}^e = C_{ijkl} d\varepsilon_{kl}^e \tag{15}$$

$$d\sigma_{ij} = C_{ijkl} d\varepsilon_{kl} - \lambda_c C_{ijkl} \frac{\partial G_c}{\partial \sigma_{kl}} - \lambda_s C_{ijkl} \frac{\partial G_s}{\partial \sigma_{kl}} - \lambda_t C_{ijkl} \frac{\partial G_t}{\partial \sigma_{kl}} \tag{16}$$

The consistency conditions for the three mechanisms are $dF_c = 0$, $dF_s = 0$ and $dF_t = 0$:

$$\begin{cases} dF_c = \frac{\partial F_c}{\partial \underline{\sigma}} d\underline{\sigma} + \frac{\partial F_c}{\partial p_c'} dp_c' = 0 \\ dF_s = \frac{\partial F_s}{\partial \underline{\sigma}} d\underline{\sigma} + \frac{\partial F_s}{\partial \varepsilon_s^p} d\varepsilon_s^p = 0 \\ dF_t = \frac{\partial F_t}{\partial \underline{\sigma}} d\underline{\sigma} + \frac{\partial F_t}{\partial \varepsilon_t^p} d\varepsilon_t^p = \frac{\partial F_t}{\partial \underline{\sigma}} d\underline{\sigma} = 0 \end{cases} \tag{17}$$

with ε_s^p the plastic distortion (plastic shear strain) which represents the internal variable relative to the shear failure; ε_t^p the plastic tensile strain. Furthermore, the consolidation stress increment is expressed as a function of the independent increments of plastic deformation related to pore collapse/thermal compaction $d\varepsilon_v^c$ and temperature:

$$dp_c' = \frac{\partial p_c'}{\partial \varepsilon_v^c} d\varepsilon_v^c + \frac{\partial p_c'}{\partial T} dT = \lambda_c \frac{\partial p_c'}{\partial \varepsilon_v^c} \frac{\partial G_c}{\partial p'} + \frac{\partial p_c'}{\partial T} dT \tag{18}$$

The combination of equations (16), (17) and (18) leads to the equation for individual mechanisms and a system of equations for mixed mechanisms summarised in Table 4. This allows for the calculation of at least one of the 3 plastic multipliers, at best two of the 3, provided in the Appendix. This determination of the plastic multipliers of the mechanisms involved allows for the evaluation of the irreversible strain increments $d\underline{\varepsilon}^s$ and $d\underline{\varepsilon}^c$ and then the increments of the reversible strain $d\underline{\varepsilon}^e$ and those of the stresses $d\underline{\sigma}$. Subsequently, the stress tensors $\underline{\sigma}$, the irreversible strains $\underline{\varepsilon}^p$ and $\underline{\varepsilon}^c$ as well as the expansion rate β,the plastic distortion ε_s^p and consolidation stress p_c' are updated.

The simplified projection algorithm of the proposed model is illustrated below (Table 5). This algorithm has been implemented as a Dynamic Link Library (*DLL*) in the latest commercial version of the finite difference calculation code *FLAC*^{3D} (7.0). In the following, we present some examples of numerical simulations on simple stress paths to verify the restitution of the implemented model. Unless otherwise stated, the simulations were performed with the values discussed above and summarised in Tables 2 and 3.

4.2 Verification on triaxial stress path

An example of instantaneous and long-term response curves of the claystone is presented in Armand et al. (2017c). The first verification of the proposed model consisted of simulating two such triaxial tests at 6 and 12 MPa confinements. The numerical model consists of loading a 76 mm high cylindrical specimen with a height-to-diameter ratio of 2 as follows: (a) an isotropic compression of value equal to the desired confinement, (b) a rise in deviatoric stress at constant strain rate in the axial direction while keeping the radial confinement constant.

Comparison between the deviatoric stress curves as a function of the axial, lateral and voluminal strains obtained experimentally and those predicted by the model is illustrated in Figure 7a, b. These figures indicate good agreement between the tests and simulations: that is to say, the numerical implementation of the proposed model makes it possible to reproduce the mechanical behaviour of the COx claystone for triaxial stress path, up to peak strength. To complete this model verification on triaxial compression stress paths, several triaxial tests with load-unload cycles were simulated at different confinements: 0, 2, 5, 10 and 25 MPa. For numerical reasons the uniaxial stress is taken equal to 0.001 MPa for the uniaxial compression test.

Figure 8 displays the evolution of the deviatoric stress depending on axial, lateral and volumetric strains showing the increase in the deviatoric stress at the elastic limit and the peak strength of the COx depending on the confining pressure. Figure 9 plots the evolution of the volumetric strain with respect to the strain in the loading direction. In particular, there is a systematic contractancy/dilatancy transition (consistent with the negative and positive values of $\boldsymbol{\beta_0}$ and $\boldsymbol{\beta_m}$) whatever the confinement. Moreover, for a given strain level, the less confined the sample is, the more it dilates.

Finally, Figure 10 is used to check the elastic limit and peak of strength results of these numerical simulations with the theoretical criteria expressed by relation (7). A perfect agreement can be observed between numerical results and analytical solutions since the relative error for peak strength is less than 0.4% and 0.6% for the elastic limit. To conclude, the proposed model correctly reproduces the triaxial stress path.

4.3 Verification on hydrostatic stress path

In this section we evaluate the response of the model in the case of hydrostatic compression loading. The geometry of the specimen is cubic with sides of 38 mm. The 3 faces (x = y = z = 0) represent planes of symmetry. The normal for the lamination is directed along the z axis. The loading consists in applying a constant and identical strain rate to the 3 other faces (x = y = z = 38 mm): this, due to the transverse isotropy of the COx claystone, would lead to a difference in stress between the isotropy plane (x, y) and its axis (z). In Figure 11a we show the evolution of the stresses (x, y and z components, mean and deviatoric stresses) as function of the volumetric deformation ($\boldsymbol{\varepsilon_{vol} = \varepsilon_v = \varepsilon_{xx} + \varepsilon_{yy} + \varepsilon_{zz} = 3\,\varepsilon_{xx}}$). In particular, it shows the isotropy of the stresses in the isotropy plane and the development of deviatoric stresses with loading, consistent with the anisotropic behaviour of the material. The exponential evolution of the consolidation stress (identical to the mean stress) with regard to the plastic volumetric strain is illustrated in Figure 11b.

As there is insufficient experimental data to identify the parameters related to the isotropic behaviour of the claystone, a sensitivity study to the rate of pore collapse under hydrostatic pressure was carried out. Two numerical values of the plastic compressibility coefficient $\boldsymbol{\vartheta}$ were chosen in relation to the reference ($\vartheta_{ref} = 850$): half and double (425 and 1700). Figure 12 shows the impact of this parameter on the evolution of stresses. In particular, an increase (respectively decrease) in plastic compressibility $\boldsymbol{\vartheta}$ increases (respectively decreases) the mean and deviatoric stresses. Similarly, an increase (respectively decrease) in $\boldsymbol{\vartheta}$ decreases (respectively decreases) the volumetric plastic deformation.

5 APPLICATION TO DRAINED HEATING TEST UNDER CONSTANT *IN-SITU* STRESS

The recent work by Braun and co-authors (Braun 2019, Braun et al. 2019, 2020 and 2021) has completed the characterisation of the thermal behaviour of COx claystone undertaken by Mohajerani et al. (2012) Mohajerani et al. (2014) and Belmokhtar et al. (2017) using a specifically-developed isotropic high-pressure cell providing temperature control and strain measurement. In particular, this work has provided a comprehensive set of transverse isotropic THM parameters capable of describing the strain and pressure variations occurring during thermal loading with the specificity of correcting strain measurements that may result from alteration of the measuring gauges and/or ambient temperature variations in the chamber that may affect the external cables (Braun et al. 2019, 2020). The COx claystone samples are tested under various heating and cooling paths under constant total stresses in drained and undrained conditions, parallel and perpendicular to the stratification. The series of constant total stress drained thermal tests performed by Braun et al. (2020) where a plastic part of the observed thermo-elasto-plastic volumetric response was mainly due to deformations perpendicular to the bedding was used to test the ability of the proposed model to reproduce the observed thermal compaction. These are the ISO3 and ISO4 tests shown in Figure 4. The pore pressure and confining stress were increased simultaneously under effective stress, until a pore pressure close to that prevailing *in situ* (i.e., 4 MPa) was reached. The ISO3 and ISO4 samples were therefore increased to 12 and 14 MPa of total stress respectively. These conditions were kept constant throughout the thermal loading. For the latter, a gradual thermal loading (rate of 7°C/h) and waiting for pore pressure dissipation were adopted according to a proven protocol (Delage et al. 2000, Braun et al. 2019). The deformation response, once stabilised at each stage, was considered representative of the drained thermal response. A maximum temperature of 90°C was applied, which is the maximum temperature allowed in the host rock (Armand et al. 2017a).

The laboratory tests showed that the thermal compaction occurs under a perfect drained condition. Then in relation to the absence of pressure and stress (effective and total) variations, the numerical simulation of the ISO3 test was carried out in the framework of thermomechanical approach with total stresses representative of the *in-situ* conditions. A quarter of the real cylindrical specimen (diameter 38 mm and height 10 mm) is modelled with two planes of symmetry P1 and P2. The first phase consists of thermomechanical consolidation at -12 MPa in stress and 25°C in temperature. The

second phase consists of thermal loading (a temperature increase at a constant rate of 0.4°C/h) with a first cooling phase (numerical) followed by a second temperature rise to about 90°C before the cooling phase. The boundary conditions applied for these two phases are summarised in Figure 13.

Figure 14b shows the evolution of the volumetric deformation depending on temperature predicted by the proposed model. The main points are: (a) the thermal compaction phenomenon observed on the COx claystone in tests by Belmokhtar et al. (2017), Braun et al. (2019, 2020, 2021) beyond a maximum temperature supported in its history is adequately reproduced. In particular, the results of the tests by Braun and co-authors (Figure 14a) were qualitatively and quantitatively reproduced, despite the absence of several tests to identify model parameters for the hydrostatic compaction mechanism or the dependence of peak strength and yield surfaces on temperature variations; (b) the loading history remains one of the key factors of this thermoplastic contraction. Numerically, it should be noted that if the sample is heated beyond its maximum temperature experienced in the COx claystone history (50°C) to 72°C, for example before the cooling phase, it will be this temperature value that will represent the new critical temperature threshold of the sample history during the next heating-cooling cycle, and so on.

We mentioned that there is very little data on hydrostatic compression and drained heating tests to correctly describe the evolution of the critical hydrostatic pressure depending on temperature and the closure of the yield surface towards the hydrostatic part. For this simulation, we propose to conduct a sensitivity study on the values of the coefficient of plastic compressibility ϑ and the coefficient of plastic thermal expansion α_T^p. Compared to the reference value of ϑ equal to 850, two other numerical values have been studied: 425 and 1700. For the coefficient of plastic thermal expansion α_T^p whose reference value is $0.006\,°C^{-1}$, two additional values were also tested: $0.06\,°C^{-1}$ and $0.0006\,°C^{-1}$. Figure 15 shows the evolution of the volumetric deformation with respect to temperature for the different parameter values ϑ and α_T^p. It can be seen that the increase of α_T^p or decrease of ϑ accelerate the compaction phenomenon. Conversely, a decrease in α_T^p or an increase in ϑ reduces the thermal compaction with a behaviour that can extend as far as thermoelastic expansion.

6 CONCLUSION

Clay formations present very favourable conditions for the long-term containment of radioactive waste due to their low hydraulic conductivity, high radionuclide retention capacity and limited fracturing in their natural state. Three clay formations have been studied in Europe as potential host rocks for the disposal of high-level long-lived radioactive waste: the Boom clay in Belgium, the Opalinus clay in Switzerland and the Callovo-Oxfordian (COx) clay formation in France. In the latter case, a deep geological disposal project called Cigéo for high-level radioactive waste (HLW) and long-lived and intermediate-level radioactive waste (IL-LLW) is underway. Its construction is envisaged for COx claystone. For the design of the HLW repository and in order to preserve the favourable properties of the COx for long-term safety, a thorough knowledge of the THM processes in the claystone is essential. In this context, several experimental studies to characterise the behaviour and THM properties of COx have been undertaken both in the laboratory and *in situ* at the Meuse/Haute-Marne underground research laboratory (LS M/HM), but also from a theoretical and numerical point of view. In particular, the role of temperature on the THM behaviour of COx claystone was highlighted: (a) the generation of pore pressure or thermal pressurisation induced by temperature variations and differential thermal expansion between the fluid and solid phases; (b) a plastic thermal compaction mechanism occurring above a temperature threshold that would correspond to the maximum temperature value experienced by the COx claystone during its history, and this contrary to the thermoelastic expansion generally observed on rocks due to thermal expansion.

Based on the little experimental data available in the literature on the thermoplastic compaction of COx claystone, the extensive literature on the thermomechanical behaviour of clay soils and clays, and the anisotropic mechanical behaviour (in situ and laboratory characterisation, failure criteria and rheological models) of COx claystone, a thermomechanical constitutive model is proposed. The main characteristics of the instantaneous behaviour of the COx claystone, which have been demonstrated experimentally and taken into account in the model, are (a) transverse isotropic elasticity, (b) elastoplasticity with positive strain hardening before failure (peak strength characterised by a Hoek-Brown type criterion), (c) a transition from contracting to expanding volumetric deformations due to shear, and (d) plastic collapse of the COx structure under the effect of hydrostatic pressure and/or

temperature from a certain threshold in effective mean stress and temperature. The model is built within the framework of a phenomenological approach, which has the advantage that it can be enriched afterwards to take into account other characteristics of the behaviour of the claystone (creep, post-peak behaviour, damage, etc.).

The proposed model is implemented in an industrial code (FLAC^{3D}) and verified on simple stress paths: triaxial and hydrostatic. In particular, the simulation of triaxial tests carried out on COx showed that the model reproduces well the non-linear behaviour of claystone until failure. As an application, the instantaneous heating tests under drained conditions by Braun et al. (2019) with prevailing *in-situ* stresses and pore pressures (12 MPa and 4 MPa respectively) were simulated. The test results of Braun et al. (2019) were qualitatively and quantitatively reproduced, despite the absence of isothermal and non-isothermal experimental hydrostatic data needed to rigorously identify the full model parameters.

This rheological study provides a basis for applications to estimate the consequences of thermal compaction on the effective stresses around the specific THM experiments of the LS M/HM laboratory (TER, CRQ, etc.) and on the design of HA cells (evolution of pore pressure and effective stresses at the ½ distance between two cells). Prior to this, the hydrostatic and thermoplastic strengths parameters of the COx claystone will be identified from characterisation tests currently being carried out in Andra's partner laboratories.

Data availability

Not applicable.

Declarations

Conflict of interest: The authors declare no competing interests.

7 REFERENCES

Abuel-Naga HM, Bergado DT, Bouazza A (2007) Thermally induced volume change and excess pore water pressure of soft Bangkok clay. Eng Geol 89:144–154

Armand G, A Noiret, J Zghondi, DM Seyedi (2013) Short- and long term behaviors of drifts in the Callovo-Oxfordian claystone at the Meuse/Haute-Marne Underground Research Laboratory. J Rock Mech Geotech Eng 5(3):221–230

Armand G, Seyedi D, Vu MN, Vitel M (2017b) Key THM processes for the design of high level waste are in the Cigéo project. 7th International Conference on Clays in Natural and Engineered Barriers for Radioactive Waste Confinement, Davos, Switzerland

Armand G, N Conil, Talandier J, Seyedi DM (2017c) Fundamental aspects of the hydromechanical behaviour of Callovo-Oxfordian claystone: from experimental studies to model calibration and validation. Comput Geotech 85:277-286

Armand G, Bumbieler F, Conil N, de La Vaissière R, Bosgiraud JM, Vu MN (2017a) Main outcomes from in situ THM experiments programme to demonstrate feasibility of radioactive HL-ILW disposal in the Callovo-Oxfordian claystone. J Rock Mech Geotech Eng 9(3):415-427

Armand G, Leveau F, Nussbaum C, de La Vaissiere R, Noiret A, Jaeggi D, Landrein P, Righini C (2014) Geometry and Properties of the Excavation-Induced Fractures at the Meuse/Haute-Marne URL Drifts. Rock Mech Rock Eng 47:21-41

Armero F, Simo JC (1993) A priori stability estimates and unconditionally stable product formula algorithms for nonlinear coupled thermoplasticity. Int J Plast 9(6):749–782

Baldi G, Hueckel T, Peano A, Pellegrini R (1991) Developments in modelling of thermo-hydro-geomechanical behaviour of Boom Clay and clay-based buffer materials. Commission of the European communities, nuclear science and technology EUR13365/2. vol. 2; 1991

Baldi G, Hueckel T, Pellegrini R (1988) Thermal volume changes of the mineral-water system in low porosity clay soils. Can Geotech J 25:807–825

Bellia Z, Ghembaza MS, Belal T (2015) A thermo-hydro-mechanical model of unsaturated soils based on bounding surface plasticity. Comput Geotech 69:58-69

Belmokhtar M, Delage P, Ghabezloo S, Conil N (2017) Thermal volume changes and creep in the Callovo–Oxfordian claystone. Rock Mech Rock Eng 50:2297–2309

Blaise T, Barbarand J, Kars M, Ploquin F, Aubourg C, Brigaud B, Cathelineau M, El Albani A, Gautheron C, Izart A, Janots D, Michels R, Pagel M, Pozzi J-P, Boiro MC, Landrein P (2014) Reconstruction of low temperature (<100 °C) burial in sedimentary basins: a comparison of geothermometer in the intracontinental Paris Basin. Mar Pet Geol 53:71–87

Blümling P, Bernier F, Lebon P, Martin C-D (2007) The excavation damaged zone in clay formations time-dependent behaviour and influence on performance assessment. Phys Chem Earth 32:588-599

Borja RI, Yin Q, Zhao Y (2020) Cam-Clay plasticity. Part IX: On the anisotropy, heterogeneity, and viscoplasticity of shale. Comput Method Appl Mech Eng 360:112695

Bossart P, Meier P-M, Moeri A, Trick T, Mayor J-C (2002) Geological and hydraulic characterisation of the excavation disturbed zone in the Opalinus Clay of the Mont Terri Rock Laboratory. 66:19-38

Bossart P, Trick T, Meier P-M, Mayor J-C (2004) Structural and hydrogeological characterisation of the excavation-disturbed zone in the Opalinus Clay (Mont Terri Project, Switzerland). Appl Clay Sci 26:429-448

Braun P, Delage P, Ghabezloo S, Sulem J, Conil N (2020) Effect of anisotropy on the thermal volume changes of the Callovo–Oxfordian claystone. Géotechnique Letters 10(1):63–66, DOI 10.1680/jgele.19.00045

Braun P, Ghabezloo S, Delage P, Sulem J, Conil N (2019) Determination of Multiple Thermo-Hydro-Mechanical Rock Properties in a Single Transient Experiment: Application to Shales. Rock Mech Rock Eng 52(7):2023-2038

Braun P, Ghabezloo S, Delage P, Sulem J, Conil N (2021) Thermo-Poro-Elastic Behaviour of a Transversely Isotropic Shale: Thermal Expansion and Pressurization. Rock Mech Rock Eng 54(1):359–375, DOI 10.1007/s00603-020-02269-y

Braun P (2019) Thermo-hydro-mechanical behavior of the Callovo-Oxfordian claystone: Effects of stress paths and temperature changes. Thèse de Doctorat de l'Université de Paris-Est

Cekerevac C, Laloui L (2004) Experimental study of thermal effects on the mechanical behavior of a clay. Int J Num Anal Meth Geomech 28:209–228

Chakraborty T, Salgado R, Loukidis D (2013) A two-surface plasticity model for clay. Comput Geotech 49:170-190

Chen G, Gallipoli D, Ledesma A (2007) Chemohydro- mechanical coupled consolidation for a poroelastic clay buffer in a radioactive waste repository. Trans Porous Media 69 (2):189-213

Cheng W, Hong P-Y, Pereira J-M, Cui Y-J, Tang AM, Chen R-P (2020) Thermo-elasto-plastic modeling of saturated clays under undrained conditions. Comput Geotech 125:1036-88

Chiarelli AS, Shao JF, Hoteit N (2003) Modeling of elastoplastic damage behavior of a claystone. Int J Plast 19:23-45

Collin F, Li X, Radu JP, Charlier R. (2002) Thermo-hydro-mechanical coupling in clay barriers. Eng Geol 64:179–93

Collins IF, Kelly PA (2002) A thermomechanical analysis of a family of soil models. Géotechnique 52(7):507-18

Conil N, Vitel M, Plúa C, Vu MN, Seyedi DM, Armand G (2020) In situ investigation of the THM behavior of the Callovo-Oxfordian claystone. Rock Mech Rock Eng. 53:2747–2769

Cui YJ, Le TT, Tang AM, Delage P, Li XL (2009) Investigating the time dependent behaviour of Boom clay under thermo-mechanical loading. Géotechnique 59(4):319-329

Cui YJ, Sultan N, Delage P (2000) A thermomechanical model for clays. Can Geotech J 37(3): 607–620

Cui YJ, Tang AM (2013) On the chemo-thermo-hydro-mechanical behaviour of geological and engineered barriers. J Rock Mech Geotech Eng 5(2013):169–178

Dafalias Y F (1986) An anisotropic critical state soil plasticity model. Mech Resear Com 13:341-347

Delage P, Sultan N, Cui YJ (2000) On the thermal consolidation of Boom clay. Can Geotech J 37(2):343–354

François B, Laloui L, Laurent C (2009) Thermo-hydro-mechanical simulation of ATLAS in situ large scale test in boom clay. Comput Geotech 36(4):624–640

François B, Laloui L (2008) ACMEG-TS: A constitutive model for unsaturated soils under non-isothermal conditions. Int J Numer Anal Methods Geomech 32:1955–1988

Garitte B, Gens A, Vaunat J, Armand G (2014) Thermal conductivity of argillaceous rocks: determination methodology using in situ heating tests. Rock Mech Rock Eng 47:111–129

Geng Z, Bonnelye A, Chen M, Jin Y, Dick P, David C, Fang X, Schubnel A (2020) Time and Temperature Dependent Creep in Tournemire Shale. Journal of Geophysical Research: Solid Earth, AGU, 123(11):9658-9675

Gens A, Potts DM (1988) Critical state models in computational geomechanics. Eng Comput 5:178-197

Gens A, Vaunat J, Garitte B, Wileveau Y (2007) In situ behaviour of a stiff layered clay subjected to thermal loading: observations and interpretation. Géotechnique 57(2):207–228

Ghabezloo S, Sulem J, Saint-Marc J (2009) The effect of undrained heating on a fluid-saturated hardened cement paste. Cement and Concrete Research 39(1):54-64

Ghabezloo S, Sulem J (2009) Stress dependent thermal pressurization of a fluid-saturated rock. Rock Mech Rock Eng 42(1):1-24

Gurson AL (1977). Continuum theory of ductile rupture by void nucleation and growth: Part I – Yield criteria and flow rules for porous ductile media. J Eng Mater Tech. 99:2–15

Hamidi A, Khazaei C (2010) A thermo-mechanical constitutive model for saturated clays. Int J Geotech Eng 4(4):445-59

Hamidi A, Tourchi S (2017) A thermo-mechanical constitutive model for unsaturated clays. Int J Geotech Eng 2017. https://doi.org/10.1080/19386362.2016.1260312.

Hamidi A, Tourchi S, Khazaei C (2015) Thermomechanical constitutive model for saturated clays based on critical state theory. Int J Geomech 15(1). https://doi.org/10.1061/(ASCE)GM.1943-5622.0000402

Hoek E, Brown ET (1980) Empirical strength criterion for rock masses. J Geotech Eng Div ASCE 106:1013–1035

Hong PY, Pereira JM, Cui YJ, Tang AM (2016) A two-surface thermomechanical model for saturated clays. Int J Numer Anal Methods Geomech 40:1059–1080

Hoxha D, Giraud A, Blaisonneau A, Homand F, Chavant C (2004) Poroplastic modelling of the excavation and ventilation of a deep cavity. Int J Numer Anal Methods Geomech 28:339–364

Hueckel T, François B, Laloui L (2009) Explaining thermal failure in saturated clays. Géotechnique 59(3):197–212

Hueckel T, Baldi G (1990) Thermoplasticity of saturated clays: experimental constitutive study. J Geotech Eng 116(12):1778–1796

Hueckel T, Borsetto M (1990) Thermoplasticity of saturated soils and shales: constitutive equations. J Geotech Eng ASCE 116(12):1765–1777

Hueckel T, Francois B, Laloui L (2011) Temperature-dependent internal friction of clay in a cylindrical heat source problem. Géotechnique 61:831-844

Khalili N, Loret B (2001) An elasto-plastic model for non-isothermal analysis of flow and deformation in unsaturated porous media: formulation. Int J Solid Struct 38:8305–8330

Lagioia R, Potts DM (1988) A new versatile expression for yield and plastic potential surfaces. Comput Geotech 5:178-197

Laloui L, Cekerevac C (2003) Thermo-plasticity of clays: An isotropic yield mechanism. Comput Geotech 30(8): 649-660

Liu Z, Li X, Tang L (2007) A Coupled Chemo- Thermo-Hydro-Mechanical Constitutive Model for Porous Media. Proc. Int Conf Comput Sci 1210-1213

Menaceur H, Delage P, Tang AM, Conil N (2016) On the Thermo-Hydro-Mechanical Behaviour of a Sheared Callovo-Oxfordian Claystone Sample with Respect to the EDZ Behaviour. Rock Mech Rock Eng 49(5):1875-1888

Mertens J, Bastiaens W, Dehandschutter B (2004) Characterisation of induced discontinuities in the Boom Clay around the underground excavations (URF, Mol, Belgium). Appl Clay Sci 26:413-428

Mohajerani M, Delage P, Sulem J, Monfared M, Tang A-M, Gatmiri B (2014) The thermal volume changes of the Callovo-Oxfordian claystone. Rock Mech Rock Eng 47:131–142

Mohajerani M, Delage P, Sulem J, Monfared M, Tang AM, Gatmiri B (2012) A laboratory investigation of thermally induced pore pressures in the Callovo-Oxfordian claystone. Int J Rock Mech Min Sci 52:112-121

Monfared M, Sulem J, Delage P, M. Mohajerani (2011) A laboratory investigation on thermal properties of the Opalinus claystone. Rock Mech Rock Eng 44:735–747

Mróz Z, Raniecki B (1976) On the uniqueness problem in coupled thermoplasticity. Int J Eng Sci 14(2):211–221

Paaswell RE (1967) Temperature effects on clay soil consolidation. J Soil Mech Found Eng ASCE 93(SM3):9–22

Picard JM (1994) Ecrouissage thermique des argiles saturées: application au stockage des déchets radioactifs. PhD thesis, Ecole nationale des ponts et chaussées-ENPC PARIS/MARNE LA VALLEE, 1994.

Rachdi S, Jahangir E, Tijani M, Serratrice J-F (2019) Critical state constitutive models and shear loading of overconsolidated clays with deviatoric hardening. Studia Geotech Mech 41(4):247–262

Rice J, Tracey D (1969) On the ductile enlargement of voids in triaxial stress fields. J Mech Phys Solids 17:201–217

Robinet JC, Rahbaoui A, Plas F, Lebon P (1996) A constitutive thermomechanical model for saturated clays. Eng Geol 41(1):145–169

Romero E, A. Gens A, Lloret A (2003) Suction effect on a compacted clay under non-isothermal conditions. Géotechnique 53(1):65–81

Samudio M (2018) Modelling of an oil well cement paste from early age to hardened state : hydration kinetics and poromechanical behavior. PhD thesis Ecole des Ponts, Paris

Semnani SJ, White JA, Borja RI (2016) Thermo-plasticity and strain localization in transversely isotropic materials based on anisotropic critical state plasticity. Int J Numer Anal Methods Geomech 40 (2016):2423–2449

Seyedi DM, Armand G, Noiret A (2017) "Transverse Action"–A model benchmark exercise for numerical analysis of the Callovo-Oxfordian claystone hydromechanical response to excavation operations. Comput Geotech 85:287-305

Simo JC, Miehe C (1992) Associative coupled thermoplasticity at finite strains: formulation, numerical analysis and implementation. Comput Method Appl Mech Eng 98(1):41–104

Sloderbach Z, Pajak J (2010) Generalized coupled thermoplasticity taking into account large strains, Part I. conditions of uniqueness of the solution of boundary-value problem and bifurcation criteria. Math Mech Solid 15(3):308–327

Souley M, Vu M-N, Armand G (2022) 3D Modelling of Excavation-Induced Anisotropic Responses of Deep Drifts at the Meuse/Haute-Marne URL. Rock Mech Rock Eng **55**:4183–4207 (2022) https://doi.org/10.1007/s00603-022-02841-8

Souley M, Armand G, Kazmierczak J-B (2017) Hydro-elasto-viscoplastic modeling of a drift at the Meuse/Haute-Marne Underground Research Laboratory (URL). Comput Geotech 85:306-320

Su K (2003) Constitutive Models for the Meuse/Haute-Marne Argillites – MODEX- REP, European Commission – Nuclear science and technology. Contract n° FIKW-CT2000-00029, 2-3

Sultan N, Delage P, Cui YJ (2002) Temperature effects on the volume change behaviour of boom clay. Eng Geol 64(2–3):135–145

Tamizdoust MM, Ghasemi-Fare O (2020) A fully coupled thermo-poro-mechanical finite element analysis to predict the thermal pressurization and thermally induced pore fluid flow in soil media. Comput Geotech 117:1032-50

Towhata I, Kuntiwattanakul P, Seko I, Ohishi K (1993) Volume change of clays induced by heating as observed in consolidation tests. Soil Found 33(4):170–83

Tvergaard V, Needleman A (1984) On the creep constrained diffusive cavitation of grain boundary facets. J Mech Phys Solid 32(5):373-393

Wileveau Y, Su K (2007) In situ thermal experiments carried out in Opalinus claystone and Callovo-Oxfordian claystones by ANDRA experiment set-up and measurement results, Clay in natural and engineered barriers for radioactive waste confinement. Conf Lille, 17-20 Sept

Xiong Y, Ye G, Zhu H, Zhang S, Zhang F (2017) A unified thermo-elasto-viscoplastic model for soft rock. Int J Rock Mech Min Sci 93:1-12

Yao YP, Zhou AN (2013) Non-isothermal unified hardening model: a thermo-elasto-plastic model for clays. Géotechnique 63 (15):1328–1345 http://dx.doi.org/10.1680/geot.13.P.035

Zhang CL, Rothfuchs T, Su K, Hoteit N (2007) Experimental Study of the thermo-hydro-mechanical behaviour of indurated Clays. Phys Chem Earth 32:957-965

Zhang C_L, Conil N, Armand G (2017) Thermal effects on clay rocks for deep disposal of high-level radioactive waste. J Rock Mech Geotech Eng 9:463-478

Zhang C-H, Armand G, Conil N, Laurich B (2019) Investigation on anisotropy of mechanical properties of Callovo-Oxfordian Claystone. Eng Geol 251:128–145

Zhang H (2018) An anisotropic plasticity clay model accounting for structural effects and overconsolidation, Geomecha GeoEng 13:1, 1-10, DOI: 10.1080/17486025.2017.1400117

Zhao Y, Semnani SJ, Yin Q, Borja RI (2018) On the strength of transversely isotropic rocks. Int J Numer Anal Methods Geomech 42:1917–1934

APPENDIX

In the presence of shear and pore collapse / thermal compaction mechanisms, the resolution of system (Table 4) leads to the following values of the two associated plastic multipliers:

$$\begin{cases} \lambda_s = \dfrac{\left(\frac{\partial F_c}{\partial \sigma_{ij}} C_{ijkl} d\varepsilon_{kl} + \frac{\partial F_c \partial p'_c}{\partial p'_c \partial T} dT\right)\left(\frac{\partial F_s}{\partial \sigma_{ij}} C_{ijkl} \frac{\partial G_c}{\partial \sigma_{kl}}\right) - \left(\frac{\partial F_s}{\partial \sigma_{ij}} C_{ijkl} d\varepsilon_{kl}\right)\left(\frac{\partial F_c}{\partial \sigma_{ij}} C_{ijkl} \frac{\partial G_c}{\partial \sigma_{kl}} - \frac{\partial F_c \partial p'_c \partial G_c}{\partial p'_c \partial \varepsilon_v^c \partial p'}\right)}{det} \\ \lambda_c = \dfrac{\left(\frac{\partial F_c}{\partial \sigma_{ij}} C_{ijkl} \frac{\partial G_s}{\partial \sigma_{kl}}\right)\left(\frac{\partial F_s}{\partial \sigma_{ij}} C_{ijkl} d\varepsilon_{kl}\right) - \left(\frac{\partial F_s}{\partial \sigma_{ij}} C_{ijkl} \frac{\partial G_s}{\partial \sigma_{kl}} - \frac{\partial F_s}{\partial \varepsilon_s^p} \frac{\partial G_s}{\partial q}\right)\left(\frac{\partial F_c}{\partial \sigma_{ij}} C_{ijkl} d\varepsilon_{kl} + \frac{\partial F_c \partial p'_c}{\partial p'_c \partial T} dT\right)}{det} \end{cases} \quad (19)$$

where *det* is expressed as follows:

$$det = \left(\frac{\partial F_c}{\partial \sigma_{ij}} C_{ijkl} \frac{\partial G_s}{\partial \sigma_{kl}}\right)\left(\frac{\partial F_s}{\partial \sigma_{ij}} C_{ijkl} \frac{\partial G_c}{\partial \sigma_{kl}}\right) - \left(\frac{\partial F_s}{\partial \sigma_{ij}} C_{ijkl} \frac{\partial G_s}{\partial \sigma_{kl}} - \frac{\partial F_s}{\partial \varepsilon_s^p} \frac{\partial G_s}{\partial q}\right)\left(\frac{\partial F_c}{\partial \sigma_{ij}} C_{ijkl} \frac{\partial G_c}{\partial \sigma_{kl}} - \frac{\partial F_c}{\partial p'_c} \frac{\partial p'_c}{\partial \varepsilon_v^c} \frac{\partial G_c}{\partial p'}\right) \quad (20)$$

In the presence of shear and tensile failure mechanisms, the resolution of the system leads to the following values of the two associated plastic multipliers:

$$\begin{cases} \lambda_t = \dfrac{\frac{\partial F_t}{\partial \sigma_{ij}} C_{ijkl} d\varepsilon_{kl}}{\frac{\partial F_t}{\partial \sigma_{ij}} C_{ijkl} \frac{\partial G_t}{\partial \sigma_{kl}}} \\ \lambda_s = \dfrac{\frac{\partial F_s}{\partial \sigma_{ij}} C_{ijkl} d\varepsilon_{kl} - \lambda_t \frac{\partial F_s}{\partial \sigma_{ij}} C_{ijkl} \frac{\partial G_t}{\partial \sigma_{kl}}}{\frac{\partial F_s}{\partial \sigma_{ij}} C_{ijkl} \frac{\partial G_s}{\partial \sigma_{kl}} - \frac{\partial F_s}{\partial \varepsilon_s^p} \frac{\partial G_s}{\partial q}} \end{cases} \quad (21)$$

For shear failure:

$$\lambda_s = \frac{\frac{\partial F_s}{\partial \sigma_{ij}} C_{ijkl} d\varepsilon_{kl}}{\frac{\partial F_s}{\partial \sigma_{ij}} C_{ijkl} \frac{\partial G_s}{\partial \sigma_{kl}} - \frac{\partial F_s}{\partial \varepsilon_s^p} \frac{\partial G_s}{\partial q}} \quad (22)$$

Pore collapse only:

$$\lambda_c = \frac{\frac{\partial F_c}{\partial \sigma_{ij}} C_{ijkl} d\varepsilon_{kl} + \frac{\partial F_c \partial p'_c}{\partial p'_c \partial T} dT}{\frac{\partial F_c}{\partial \sigma_{ij}} C_{ijkl} \frac{\partial G_c}{\partial \sigma_{kl}} - \frac{\partial F_c \partial p'_c \partial G_c}{\partial p'_c \partial \varepsilon_v^c \partial p'}} \quad (23)$$

For tension:

$$\lambda_t = \frac{\frac{\partial F_t}{\partial \sigma_{ij}} C_{ijkl} d\varepsilon_{kl}}{\frac{\partial F_t}{\partial \sigma_{ij}} C_{ijkl} \frac{\partial G_t}{\partial \sigma_{kl}} - \frac{\partial F_t}{\partial \varepsilon_v^t} \frac{\partial G_t}{\partial p'}} = \frac{\frac{\partial F_t}{\partial \sigma_{ij}} C_{ijkl} d\varepsilon_{kl}}{\frac{\partial F_t}{\partial \sigma_{ij}} C_{ijkl} \frac{\partial G_t}{\partial \sigma_{kl}}} \quad (24)$$

Example of case where two distinct mechanisms are active

There are no singularity problems here, since the five domains (Fig. 6a) are distinct, leading to a unique determination of the plastic multipliers associated to each one and analytically expressed as a function of the partial derivatives of the yield surfaces and plastic potentials.
To illustrate the volumetric strain increment decomposition, let us consider domain 2. Two mechanisms occur with the associated two plastic multipliers (Eq. 19): (a) pore collapse leading to a volumetric plastic contraction ($\Delta\varepsilon_v^c < 0$) and (b) shear-induced volumetric plastic strain with a component that can be contraction ($\Delta\varepsilon_v^s < 0$) or dilation ($\Delta\varepsilon_v^s > 0$) depending on the dilatancy rate, $\beta(\varepsilon_s^p)$, expressed in relation (9). Then, the increment of the total volumetric strain is: $\Delta\varepsilon_v = \Delta\varepsilon_v^e + \Delta\varepsilon_v^c + \Delta\varepsilon_v^s$. All these cumulative volumetric strain components are available as output (print and plot). The same is done in domain 4 where Eq. (21) allows to compute the associated plastic multipliers,

and then the corresponding increment of volumetric strains. Finally, since domains 2 and 4 are disconnected, there are no pore collapse and tensile mechanisms occurring at the same time.

Table 1 - Example of expressions for $\Theta_1(T)$ and $\Theta_2(T)$ encountered in the literature

	$\Theta_1(T)$	$\Theta_2(T)$
Hueckel and Borsetto (1990), Baldi et al. (1991)	$exp\left(-\alpha_0 \Delta T \frac{\varepsilon_v^c}{\lambda^p}\right)$ α_0 a constant	$\Theta_2(T) = 2(a_1 \Delta T + a_2 \Delta T^2)$ α_1 and α_2 2 constants
Picard (1994) continued by Hong et al. (2016)	$exp(-\alpha_0 T)$ α_0 a constant	0
Semnani et al. (2016), Zhao et al. (2018) (Laloui and Cekerevac 2003 normalized with respect to T)	$\left[1 - \gamma_T \, ln\left(1 + \frac{(T - T_{ref})}{T_{ref} - 273}\right)\right]$ T and T_{ref} current and reference temperatures in Kelvin	0

Table 2 – Mean values of Hoek and Brown constants at the elastic limit and peak

Tension and shear mechanisms					**Pore collapse and thermal compaction mechanisms**	
	Initiation (i)	Peak (p)	Dilatancy			
σ_c **(MPa)**	7.4	33.5	$\boldsymbol{\beta_0}(-)$	-0.1	$\boldsymbol{p'_{c0}}$ $(\boldsymbol{MPa})$	11
m (-)	2.4	2.2	$\boldsymbol{\beta_m}(-)$	0.5	$\boldsymbol{\vartheta}(-)$	850
s (-)	1	0.3	$\boldsymbol{b_\beta}(-)$	600	$\boldsymbol{\alpha_T^p}(-)$	6x10^{-3}
σ_t **(MPa)**	$^{s}\sigma_c/_m$	$^{s}\sigma_c/_m$	$\boldsymbol{\gamma^{ult}}(\%)$	0.825	$\boldsymbol{T_c}(°\boldsymbol{C})$	50

Table 3 – Thermoelastic properties of the COx claystone

Property (Unit)	**Numerical value**
Young's modulus (GPa) : $E_\perp$, $E_{//}/E_\perp$	4, 1.5
Poisson's coefficient (-) : $\nu_{//}$, $\nu_{//\perp}$	0.3, 0.25
$\boldsymbol{G}_{//\perp} = \frac{\boldsymbol{E}_{//}\boldsymbol{E}_\perp}{(\boldsymbol{1+2\nu}_{//\perp})\boldsymbol{E}_{//}+\boldsymbol{E}_\perp}$ (GPa)	1.8
Porosity (-) n	0.19
Thermal conductivity (W/m/K) : $\lambda_\perp$, ($\lambda_{//}/\lambda_\perp$)	1.25, (1.5)
Specific heat (J/kg/K) C_p	978
Linear thermal expansion coefficient (1/K) α (x10^{-5})	1.28

Table 4 - Equations and system of equations for the 3 plastic multipliers

Single pore collapse / thermal compaction mechanism	$\frac{\partial F_c}{\partial \sigma_{ij}}\left(C_{ijkl}d\varepsilon_{kl} - \lambda_c C_{ijkl}\frac{\partial G_c}{\partial \sigma_{kl}}\right) + \frac{\partial F_c}{\partial p'_c}\left(\lambda_c \frac{\partial p'_c}{\partial \varepsilon_v^c}\frac{\partial G_c}{\partial p'} + \frac{\partial p'_c}{\partial T}dT\right) = 0$
Single shear mechanism	$\frac{\partial F_s}{\partial \sigma_{ij}}\left(C_{ijkl}d\varepsilon_{kl} - \lambda_s C_{ijkl}\frac{\partial G_s}{\partial \sigma_{kl}}\right) + \lambda_s \frac{\partial F_s}{\partial \varepsilon_s^p}\frac{\partial G_s}{\partial q} = 0$
Single tension mechanism	$\frac{\partial F_t}{\partial \sigma_{ij}}\left(C_{ijkl}d\varepsilon_{kl} - \lambda_t C_{ijkl}\frac{\partial G_t}{\partial \sigma_{kl}}\right) = 0$
Both shear and tension mechanisms	$\begin{cases} \frac{\partial F_t}{\partial \sigma_{ij}}\left(C_{ijkl}d\varepsilon_{kl} - \lambda_t C_{ijkl}\frac{\partial G_t}{\partial \sigma_{kl}}\right) = 0 \\ \frac{\partial F_s}{\partial \sigma_{ij}}\left(C_{ijkl}d\varepsilon_{kl} - \lambda_s C_{ijkl}\frac{\partial G_s}{\partial \sigma_{kl}} - \lambda_t C_{ijkl}\frac{\partial G_t}{\partial \sigma_{kl}}\right) + \lambda_s \frac{\partial F_s}{\partial \beta}\frac{\partial \beta}{\partial \varepsilon_s^p}\frac{\partial G_s}{\partial q} = 0 \end{cases}$
Both shear and mechanical/thermal compaction mechanisms	$\begin{cases} \lambda_s \frac{\partial F_c}{\partial \sigma_{ij}} C_{ijkl}\frac{\partial G_s}{\partial \sigma_{kl}} + \lambda_c\left(\frac{\partial F_c}{\partial \sigma_{ij}} C_{ijkl}\frac{\partial G_c}{\partial \sigma_{kl}} - \frac{\partial F_c}{\partial p'_c}\frac{\partial p'_c}{\partial \varepsilon_v^c}\frac{\partial G_c}{\partial p'}\right) = \frac{\partial F_c}{\partial \sigma_{ij}} C_{ijkl}d\varepsilon_{kl} + \frac{\partial F_c}{\partial p'_c}\frac{\partial p'_c}{\partial T}dT \\ \lambda_s\left(\frac{\partial F_s}{\partial \sigma_{ij}} C_{ijkl}\frac{\partial G_s}{\partial \sigma_{kl}} - \frac{\partial F_s}{\partial \varepsilon_s^p}\frac{\partial G_s}{\partial q}\right) + \lambda_c \frac{\partial F_s}{\partial \sigma_{ij}} C_{ijkl}\frac{\partial G_c}{\partial \sigma_{kl}} = \frac{\partial F_s}{\partial \sigma_{ij}} C_{ijkl}d\varepsilon_{kl} \end{cases}$

Table 5 - Simplified flowchart for the numerical implementation of the proposed model from step (n) to (n+1)

Input: 1°) $\underline{\sigma}$, $\underline{\varepsilon}^p$, $\underline{\varepsilon}^c$, p'_c, β, ε_s^p and ε_t^p at step n

2°) $\Delta\underline{\varepsilon}$ increment of total strain (without thermoelastic) at step (n+1)

ΔT current increment of temperature

Output: $\underline{\sigma}$, $\underline{\varepsilon}^p$, $\underline{\varepsilon}^c$, p'_c, β, ε_s^p and ε_t^p at step (n+1)

1. Compute the « guest » effective stresses: $\underline{\sigma} \leftarrow \Delta\underline{\sigma} + \underline{\underline{C}}:\Delta\underline{\varepsilon}$
2. Compute the yield functions F_c(eq. 4), F_s(eq. 7) and F_t(eq. 10)
3. If at least one of the 3 yield functions are positive, then:
    a. Compute the corresponding partial derivatives and plastic multiplier (see appendix for expressions)
    b. Compute the increments of irreversible and elastic strains
    c. Update the state and internal variables with respect to the effective mechanisms: $\underline{\sigma}$, $\underline{\varepsilon}^p$, $\underline{\varepsilon}^c$, p'_c, β, ε_v^c, ε_s^p and ε_t^p
4. Go to step (n+1)

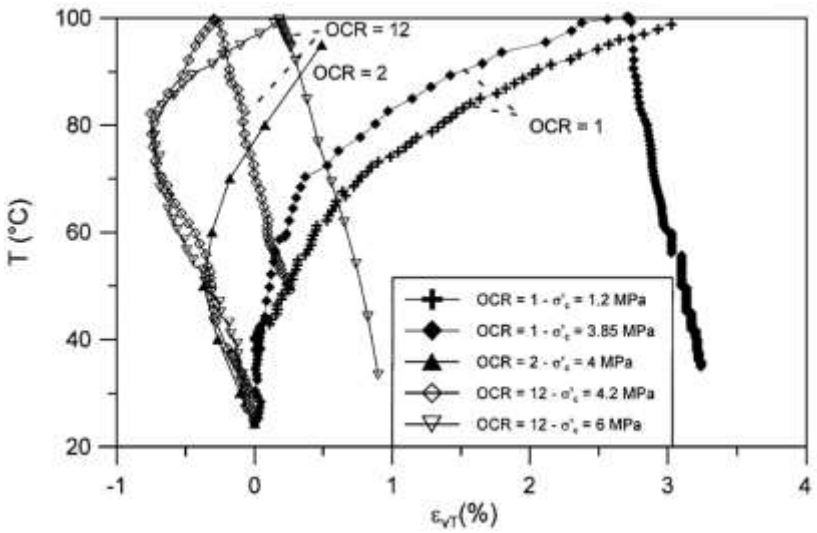

Figure 1 - Volume change during a heating-cooling cycle on Boom clay with different OCR values (after Sultan et al. 2002)

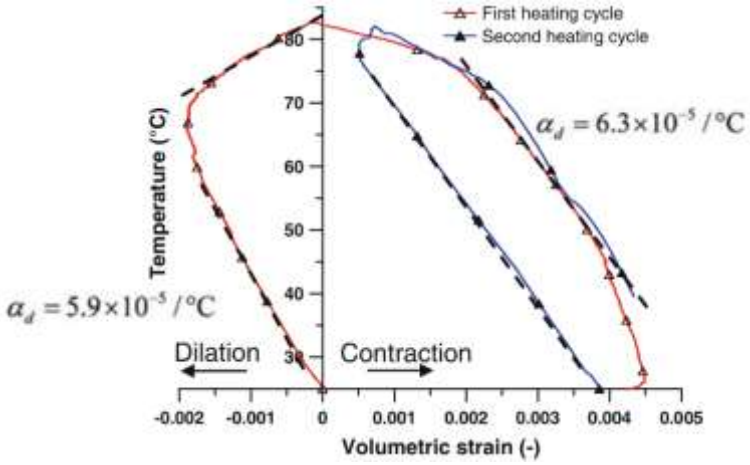

Figure 2 - Drained test with two heating / cooling cycles on Opalinus claystone (after Monfared et al. 2011)

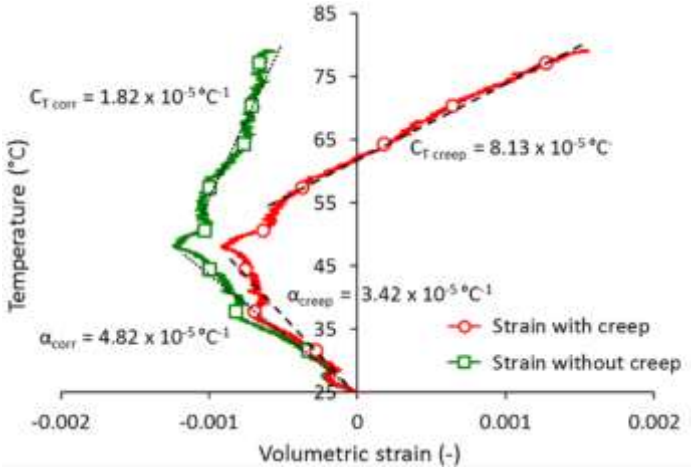

Figure 3 - Drained heating test under constant total stresses (close to those prevailing in situ) carried out on a COx sample (after Belmokhtar et al. 2017) – time-dependent versus instantaneous behaviour

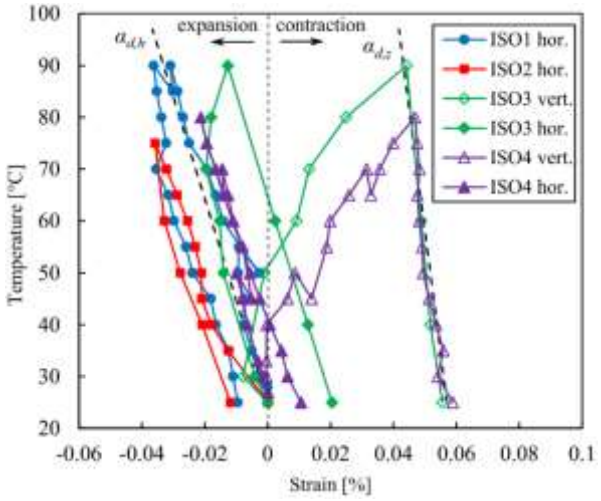

Figure 4 - Experimental results of drained heating tests carried out perpendicular (ver.) and parallel (hor.) to the bedding plane (after Braun et al. 2021)

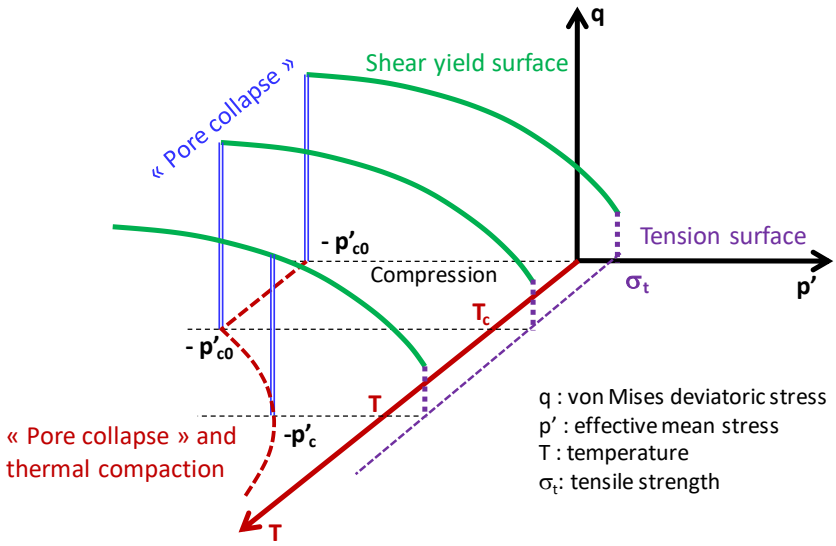

Figure 5 - Multi-mechanism yield surfaces and hardenings for the proposed thermoplastic constitutive model

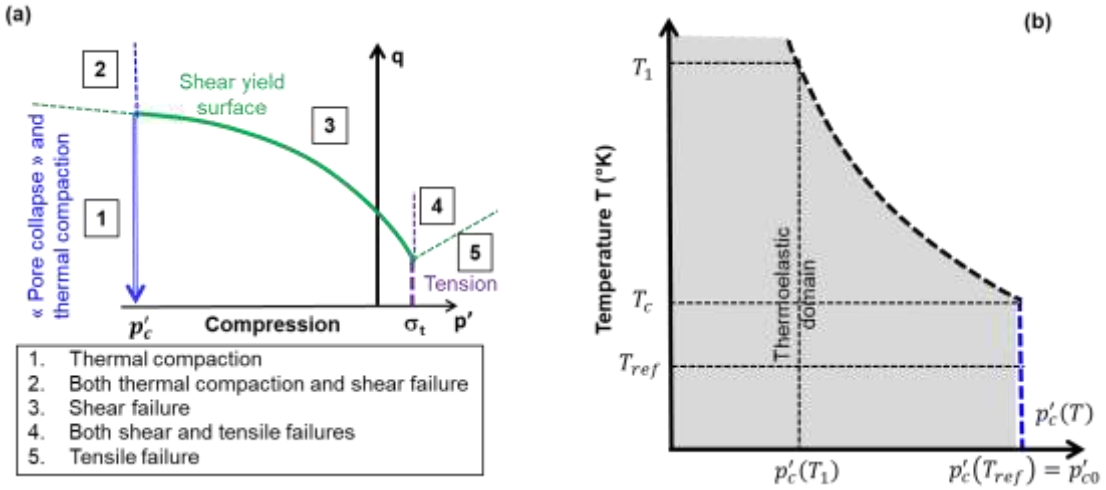

Figure 6 - (a) Illustration of current isothermal yield surfaces - stress space decomposition according to the mechanisms (b) hydrostatic and thermal compaction yield surfaces and thermoelastic domain

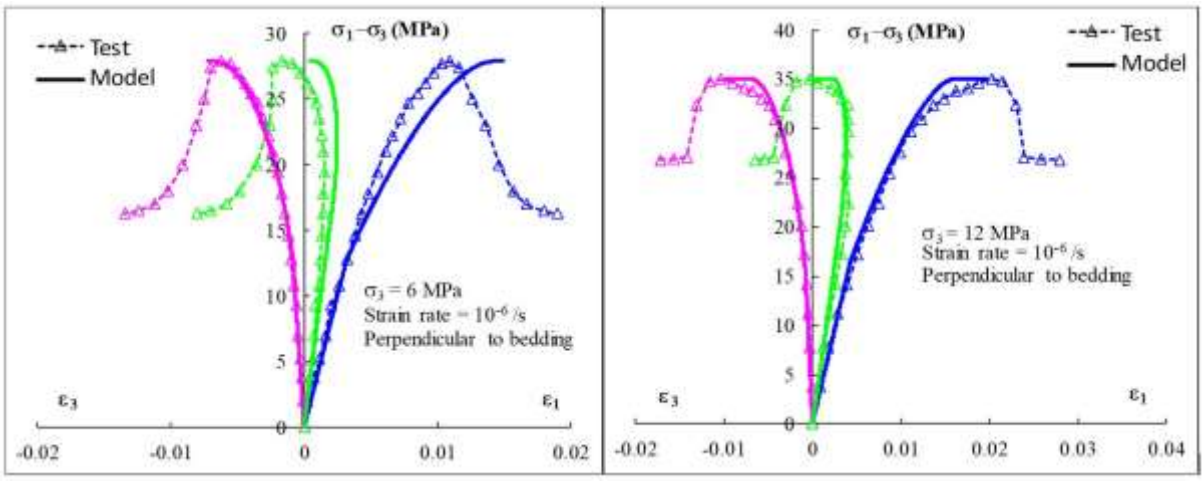

Figure 7 - Deviatoric stress vs axial (ε_1) and lateral (ε_3) strains: (a) confining pressure of 6 MPa; (b) confining pressure of 12 MPa. Laboratory tests (after Armand et al. 2017c) versus numerical simulations

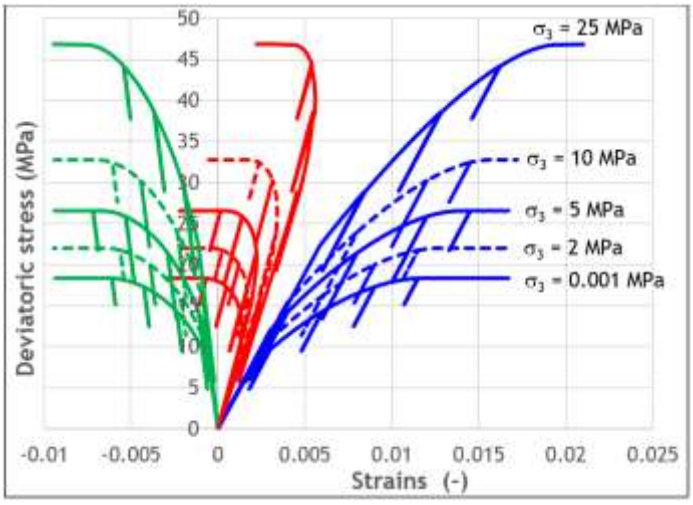

Figure 8 – Simulation of triaxial compression tests with loading-unloading cycles for confining pressure ranged from 0.001 to 25 MPa – deviatoric stress vs axial, lateral and volumetric strains

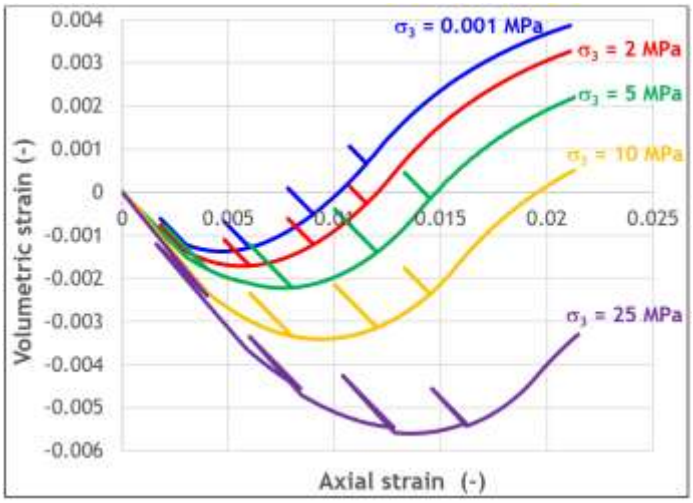

Figure 9 – Simulation of triaxial compression tests with loading-unloading cycles for confining pressure ranged from 0 to 25 MPa – volumetric strain versus axial strain

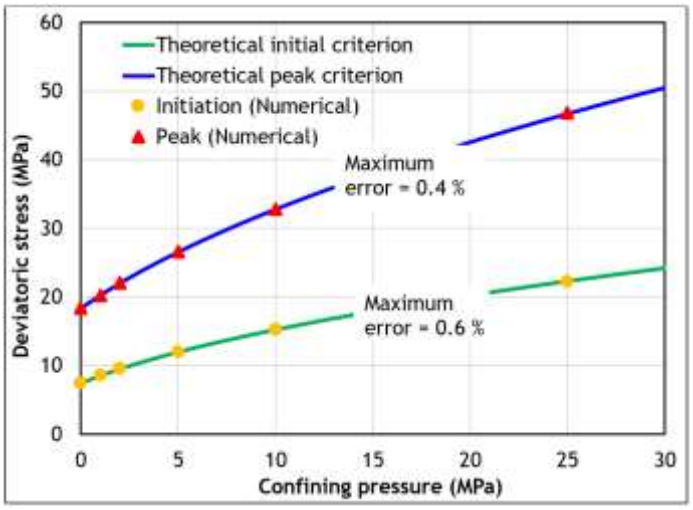

Figure 10 – Numerical verification for elastic limit and peak strength: numerical and theoretical solutions

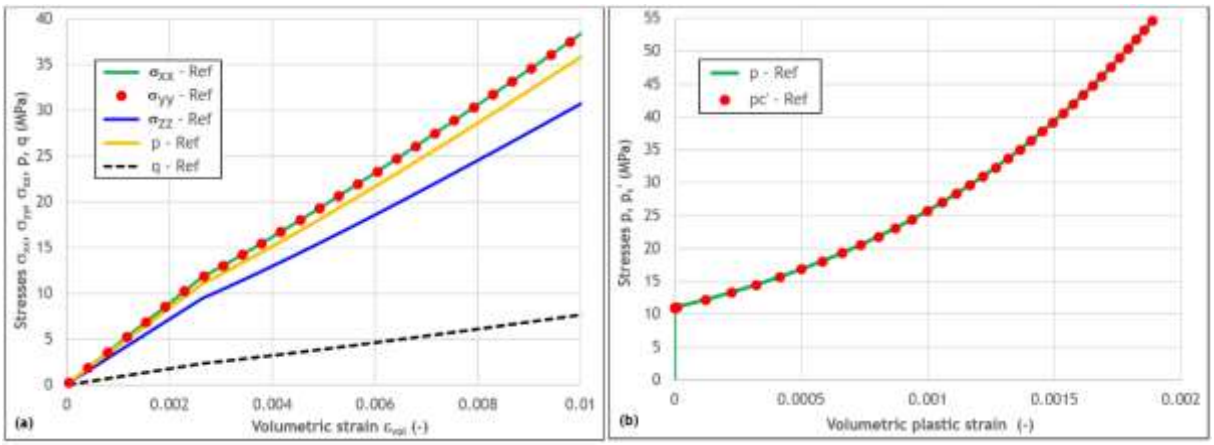

Figure 11 – Simulation of isotropic compression tests: (a) stresses vs volumetric strain, (b) mean stress and consolidation pressure as function of volumetric plastic strain

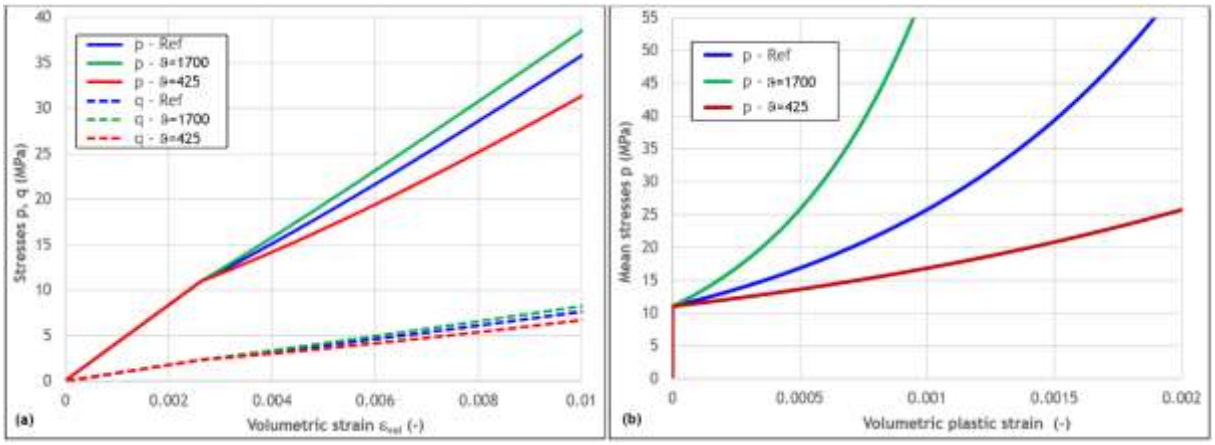

Figure 12 – Simulation of isotropic compression test – effect of plastic compressibility: (a) mean and deviatoric stresses vs volumetric strain, (b) mean stress vs volumetric plastic strain

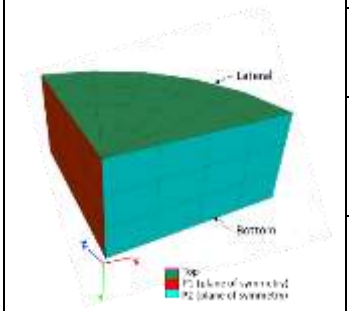

		Mechanics		Heat transport		
		Normal velocity	Normal stress	Null flux	Fixed temperature	Heating rate (± 0.4°C/h)
	Phase 1 (consolidation)	Fixed to 0 for P1, P2 and bottom	Fixed to -12 MPa for top and lateral boundaries	Planes P1 and P2	To 25°C at bottom, top and lateral boundaries	-
	Heat loading	Fixed to 0 for P1, P2 and bottom	Fixed to -12 MPa for top and lateral boundaries	Planes P1 and P2		At bottom, top and lateral boundaries

Figure 13 – Thermomechanical boundary conditions for numerical simulation

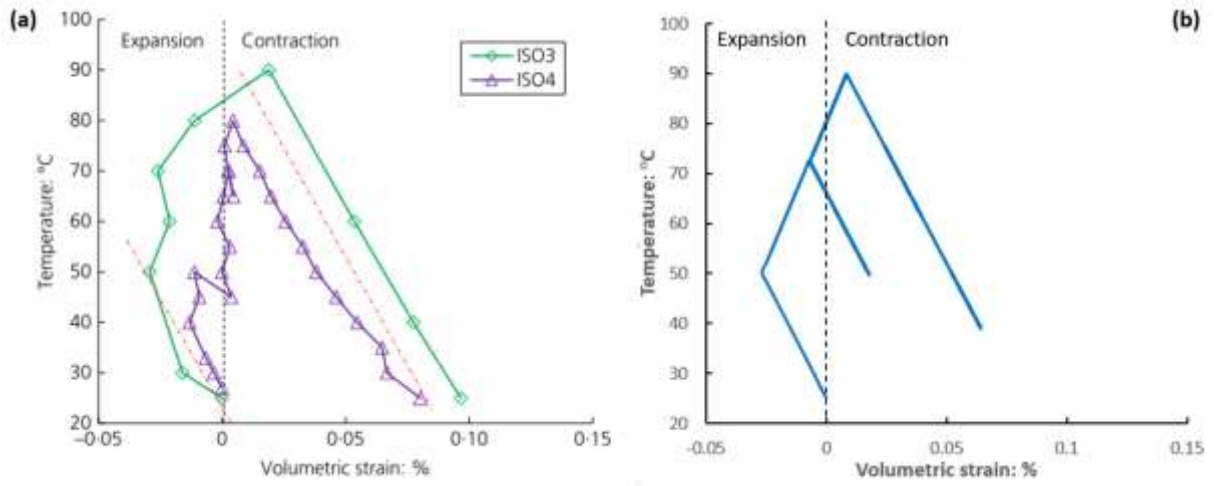

Figure 14 – (a) Drained strain changes (vertical = perpendicular and horizontal = parallel to bedding) with respect to temperature changes, under constant isotropic stresses (tests ISO3 and 4 carried out perpendicular to the bedding, after Braun et al. 2020); (b) numerical simulation of thermal compaction mechanism

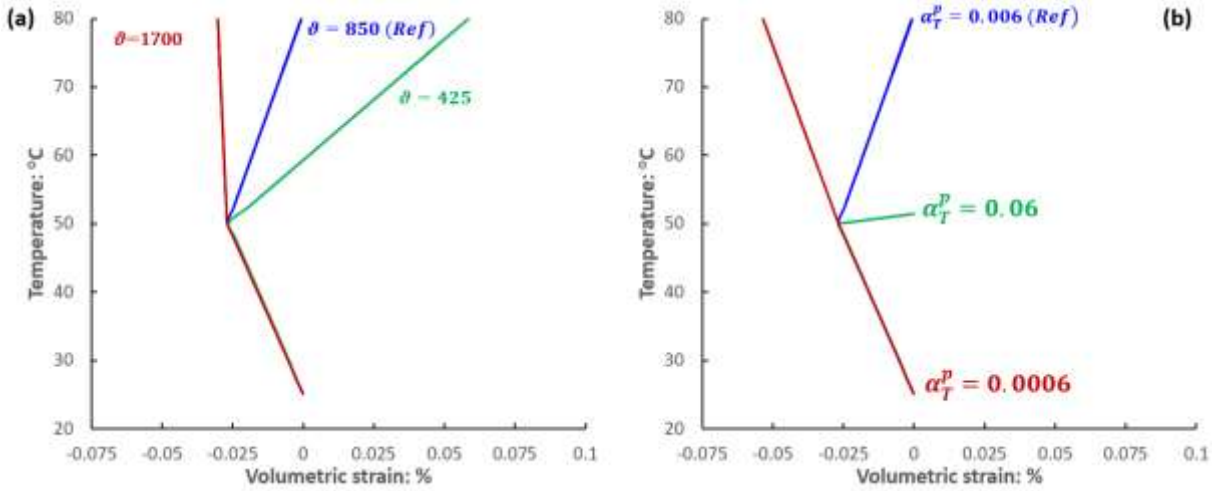

Figure 15 – Sensibility analysis on the input parameters (a) plastic compressibility ϑ_T and (b) thermal plastic expansion coefficient α_T^p